Photoinduced electron-transfer within osmium(II) and ruthenium(II) *bis*-terpyridine donor acceptor dyads†

Elvin A. Alemán, Carol D. Shreiner,‡ Cheruvallil S. Rajesh, Timothy Smith, Shana A. Garrison and David A. Modarelli*

Received 16th February 2009, Accepted 20th May 2009
First published as an Advance Article on the web 6th July 2009
DOI: 10.1039/b903130h

The synthesis and photophysical characterization of two different series of electron donor–acceptor dyads containing Ru(II) and Os(II) bis-terpyridines ($M(tpy)_2^{2+}$) were prepared and studied in order to compare the oft-studied $Ru(tpy)_2^{2+}$ chromophore with the less studied $Os(tpy)_2^{2+}$ chromophore. The first series of dyads incorporates a benzoquinone (BQ) group as the electron acceptor, whereas the second contains a substituted pyromellitimide (PI) group as the electron acceptor. Steady-state emission experiments indicated efficient quenching of the ^{3}MLCT emission of the electronically excited Os(II)-BQ complexes (**7–8**) compared to both model complexes (**3–4**) and the Os(II)-PI complex **10**. Femtosecond pump–probe absorption experiments on **7–8** yielded ultrafast electron transfer rate constants (k_{ET}) of ~2.0×10^{11} s^{-1} (**7**) and 1.3×10^{10} s^{-1} (**8**) that were in good agreement with the low emission quantum yield results. Charge-recombination (k_{CR}) in these complexes was also quite rapid, with rate constants of ~6.7×10^{10} s^{-1} (**7**) and 1.2×10^{10} s^{-1} (**8**). The analogous Ru(II) complexes underwent charge separation with rate constants of 7.6×10^{10} s^{-1} (**5**) and ~2.3×10^{10} s^{-1} (**6**), while charge recombination in these complexes occurred with rate constants of ~2.1×10^{10} s^{-1} (**5**) and ~5.3×10^{10} s^{-1} (**6**). Electron transfer in the pyromellitimide-containing complexes occurred only for Os(II)-PI (**10**), which exhibited significantly slower electron transfer (~4.3×10^6 s^{-1}) and charge recombination (~7.7×10^6 s^{-1}) rate constants. The nearly thermoneutral free energy of electron transfer and short excited state lifetime in the case of Ru(II)-PI (**9**) presumably prevents electron transfer in this compound.

Introduction

Electronic excitation of the "special pair" of chlorophylls in the photosynthetic reaction center (PRC) leads to electron-transfer to a quinone acceptor.[1] The process involves a cascade mechanism wherein several short range, ultrafast electron-transfer steps lead to highly efficient electron-transport over long distances. The reaction center in green plants is ultimately returned to its neutral, pre-photolysis state upon reduction of the oxidized special pair by the oxygen-evolving complex,[2] that in turn leads to the conversion of water to molecular oxygen.[1] The potential for converting solar energy into chemical potential by sequential electron-transfer has powered research in artificial photosynthesis for some time, and molecular systems that mimic the electron-transfer relay in photosynthesis have been studied from the joint perspectives of understanding the factors that influence photosynthesis,[1–5] as well as for their potential as alternative fuel sources.[6] Keeping in mind the high efficiency with which the sequential charge-separation in the PRC occurs, one goal in artificial photosynthesis is to generate highly efficient and sustained charge-separation for such durations that the resulting chemical potential can be realized. Molecular arrays designed to mimic the electron-transfer (ET) properties of photosynthetic organisms containing a wide variety of electron-donor (D) and electron-acceptor (A) groups have therefore been synthesized, and their properties have been studied by time-resolved spectroscopic techniques.

The use of polypyridine-transition metal complexes in photosynthetic mimics has historically focused on ruthenium(II) polypyridine complexes,[7–10] and in particular ruthenium(II) *tris*-bipyridine ($Ru(bpy)_3^{2+}$). The characteristics of $Ru(bpy)_3^{2+}$ that make it desirable for light induced processes include: (a) a low energy triplet metal-to-ligand charge-transfer state (^{3}MLCT, E_T ~2.10 eV),[11] (b) a low oxidation potential ($E_{1/2}$ ~1.26 V *vs.* SCE)[12] and (c) a long-lived excited state lifetime (τ_T ~850 ns).[5,13] Incorporation of the $Ru(bpy)_3^{2+}$ group into an array for photoinduced processes, however, is sometimes inconvenient because substitution at the 4-position on the bipyridine ligand decreases the symmetry of the metal *tris*-bipyridine, leading to geometric isomers for doubly substituted complexes.[14,15] Importantly, only the *trans* isomer has the proper orientation for keeping the donor–acceptor distance at its maximum; *cis* isomers have short D–A distances that can then lead to more rapid charge-recombination. 4′-Substituted terpyridines, on the other hand, are symmetric and can be used to prepare linear disubstituted metal complexes that can be readily extended into well-ordered arrays. The physical properties of these complexes are similar in some respects to those of the metal bipyridyl complexes. For example, both the values of the first oxidation potential and the triplet MLCT energy of ruthenium(II) *bis*-4′-methylterpyridine ($Ru(mtpy)_2^{2+}$, $E_{1/2}$ ~1.33 V[16] *vs.* SCE and E_T ~1.97 eV) are similar to those of $Ru(bpy)_2^{2+}$ ($E_{1/2}$ ~1.26 V[9]

Department of Chemistry and The Center for Laser and Optical Spectroscopy, Knight Chemical Laboratory, The University of Akron, Akron, OH 44325-3601, USA

† Electronic supplementary information (ESI) available: Experimental details. See DOI: 10.1039/b903130h

‡ Present address: Hiram College, Hiram, OH 44234

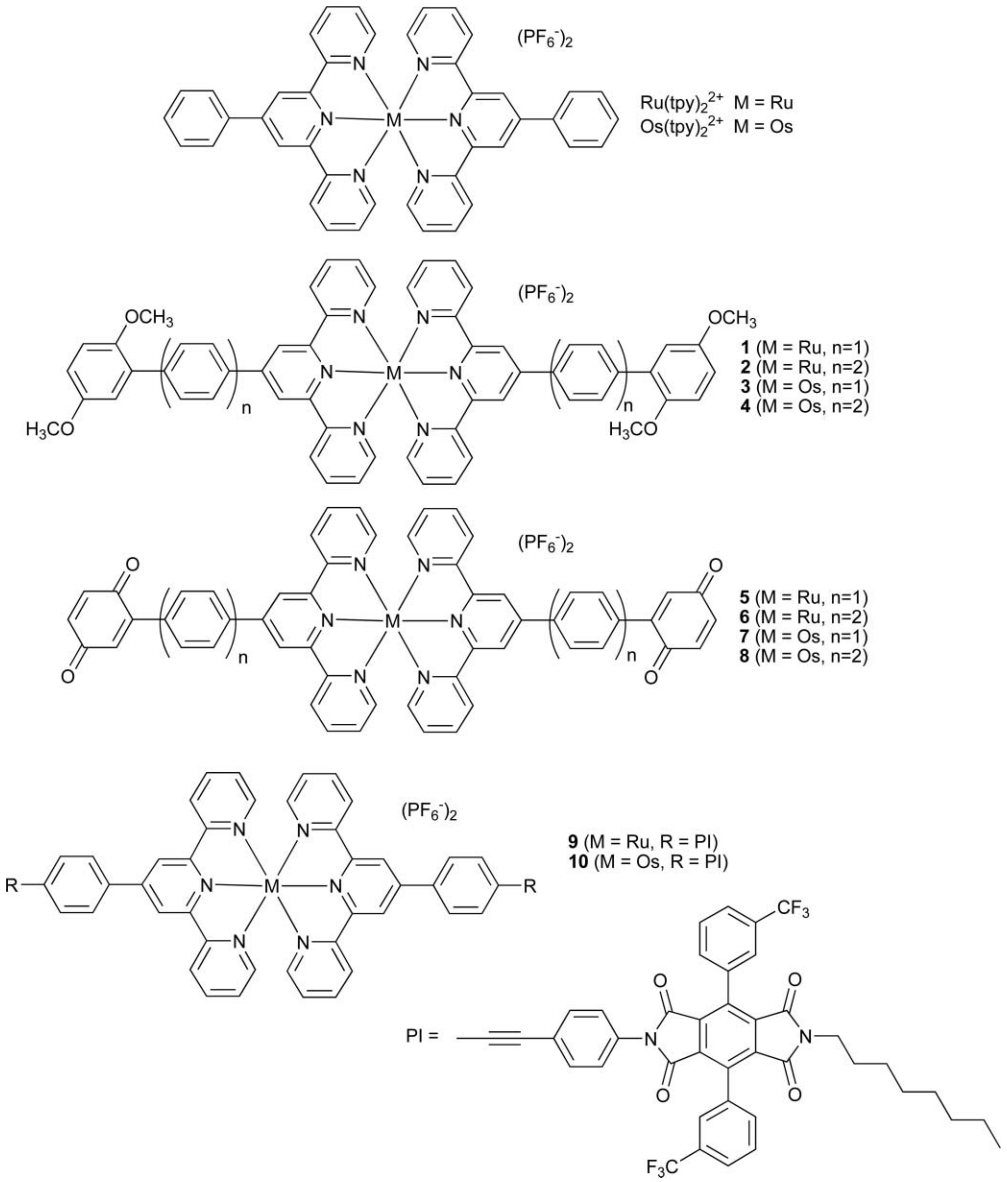

Chart 1

vs. SCE and E_T ~2.10 eV[8]). Changing the polypyridine ligands from bipyridines to terpyridines, however, dramatically decreases both the emission lifetime and quantum yield of the ^{3}MLCT state. Thus, the ^{3}MLCT excited state lifetime decreases from τ_T ~850 ns[5] for $Ru(bpy)_3^{2+}$ to ~40 ps[12,17] for $Ru(mtpy)_2^{2+}$ and 740 ps[18,22] for $Ru(ttpy)_2^{2+}$, while Φ_{em} decreases from ~1.0 for $Ru(bpy)_3^{2+}$ to nearly zero in both Ru-bisterpyridines.[18] The short-lived ^{3}MLCT state for the Ru-bisterpyridines generally results in inefficient photoinduced ET, and trade offs clearly exist when choosing between $Ru(bpy)_3^{2+}$ and $Ru(tpy)_2^{2+}$ complexes in artificial photosynthetic applications.

The use of osmium(II) bisterpyridines ($Os(tpy)_2^{2+}$) has not been as well documented in solar energy conversion schemes compared to $Ru(bpy)_3^{2+}$ and $Ru(tpy)_2^{2+}$, in part because of the more drastic synthetic conditions necessary for the preparation of the osmium complexes. The synthesis of $Os(tpy)_2^{2+}$ complexes generally requires either high temperatures (*i.e.*, 80–200 °C) or strongly acidic conditions, both of which can interfere with a variety of functional groups.[19] Nonetheless, $Os(tpy)_2^{2+}$-containing complexes possess certain advantages over both $Ru(bpy)_3^{2+}$ and $Ru(tpy)_2^{2+}$-containing complexes. For example, the ^{3}MLCT state of $Os(tpy)_2^{2+}$ is both higher in energy (1.69 eV *vs*. 1.33 eV[v]) and has a longer lived ^{3}MLCT lifetime (*i.e.*, τ_T ~220 ns *vs*. 40 ps[17]) than $Ru(tpy)_2^{2+}$. An important implication of the higher energy ^{3}MLCT state in $Os(tpy)_2^{2+}$ complexes is that triplet energy transfer in these complexes is less significant than in $Ru(bpy)_3^{2+}$ or $Ru(tpy)_2^{2+}$, and ET consequently competes more efficiently with energy-transfer in dyads containing these chromophores. Osmium *bis*-terpyridines may therefore prove useful for driving photoinduced redox reactions that do not readily occur with the less reducing and shorter-lived $Ru(tpy)_2^{2+}$ complexes. In order to assess the properties of $Os(tpy)_2^{2+}$ complexes as electron-donors we prepared both $Os(tpy)_2^{2+}$ and $Ru(tpy)_2^{2+}$ complexes covalently bound to electron-acceptor groups. In this paper we describe the synthesis and detailed photophysical properties of $Os(tpy)_2^{2+}$

containing complexes having either dimethoxybenzene (DMB, **3–4**), benzoquinone (BQ, **7–8**) and pyromellitimide (PI, **10**) groups, and compare their photophysical properties to the Ru-containing analogs (**1–2**, **5–6** and **9**).

Results and discussion

Synthesis

The synthesis of terpyridine ligands **11–12** and **15–16** was accomplished through the reaction sequence shown in Scheme 1. Condensation of 2-acetylpyridine with 1.0 M NaOH and either benzaldehyde or 4-iodobenzaldehyde, followed by refluxing with acetic acid and ammonium acetate yielded 4′-phenylterpyridine **11** and 4′-(4-iodophenyl) terpyridine **12** (Scheme 1).[20] Reaction of **12** under Suzuki coupling conditions[21] with either 2,5-dimethoxyphenyl boronic acid **13** or 4-(2′,5′-dimethoxyphenyl)-phenyl boronic acid **14** yielded dimethoxybenzene-containing terpyridines **15** and **16**, respectively.

Ruthenium complexes $Ru(phtpy)_2^{2+}$ and **1–2** were prepared by refluxing two equivalents of the appropriate terpyridine (*e.g.*, **11**, **15–16**) with $RuCl_3 \cdot 3H_2O$ in ethanol (Scheme 2).[22] The corresponding osmium complexes ($Os(phtpy)_2^{2+}$, **3–4**) were similarly prepared by refluxing $OsCl_3 \cdot 3H_2O$ with two equivalents of the terpyridine in ethylene glycol. Complexes **1–4** were fully characterized by NMR, IR and ESI–MS. Conversion of the dimethoxybenzene-containing complexes to the corresponding benzoquinone-containing dyads (**5–8**) was accomplished by demethylation of **1–4** with BBr_3[23] followed by oxidation with DDQ.

The synthesis of diimide-containing complexes **9–10** was accomplished as shown in Scheme 3. Dianhydride **17**[24] was reacted with *p*-iodoaniline and octylamine in DMF to form **18**, which was subsequently reacted with 4′-ethynylphenylterpyridine **19**[25] under modified Sonogoshira conditions[26] to yield diimide-containing terpyridine **20**. Symmetric dyads **9** and **10** were prepared by reaction of **20** with $RuCl_3 \cdot 3H_2O$ or $OsCl_3 \cdot 3H_2O$, respectively.

Absorption spectroscopy

The absorption spectra of ruthenium complexes $Ru(phtpy)_2^{2+}$, **1**, **2**, **5**, **6** and **9** in DMF (Fig. 1, Table 1) are characterized by the allowed singlet metal-to-ligand charge-transfer (^{1}MLCT) transition at λ_{MLCT} ~498–500 nm (Table 1) and a higher energy ligand centered (LC) $\pi \rightarrow \pi^*$ transition at λ_{LC} ~332–336 nm. Osmium-containing complexes $Os(phtpy)_2^{2+}$, **3**, **4**, **7**, **8** and **10** in DMF are also characterized by the presence of the ^{1}MLCT band at λ_{MLCT} ~497–501 nm and the LC $\pi \rightarrow \pi^*$ transition at λ_{LC} ~318–320 nm, but have an additional absorption at ~671–678 nm arising from the forbidden triplet MLCT (^{3}MLCT) transition (Fig. 2, Table 1). The ^{1}MLCT bands in **1–10** are all red-shifted by

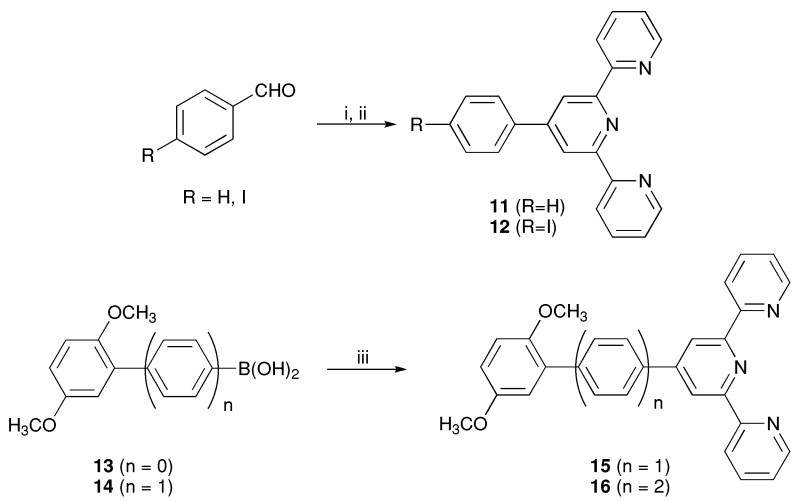

(i) 2-Acetylpyridine, NaOH, EtOH, (ii) NH_4OAc, HOAc, (iii) **12** (R = I), $Pd(Ph_3P)_4$, K_2CO_3, DME, H_2O

Scheme 1

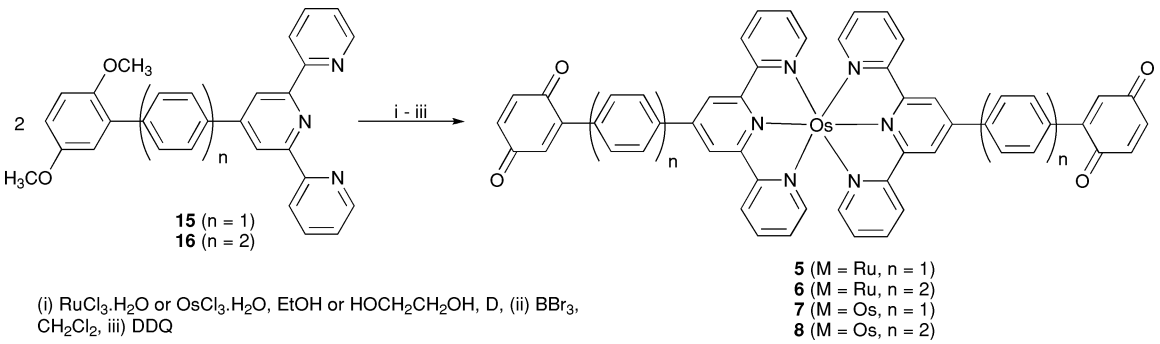

(i) $RuCl_3.H_2O$ or $OsCl_3.H_2O$, EtOH or $HOCH_2CH_2OH$, D, (ii) BBr_3, CH_2Cl_2, iii) DDQ

Scheme 2

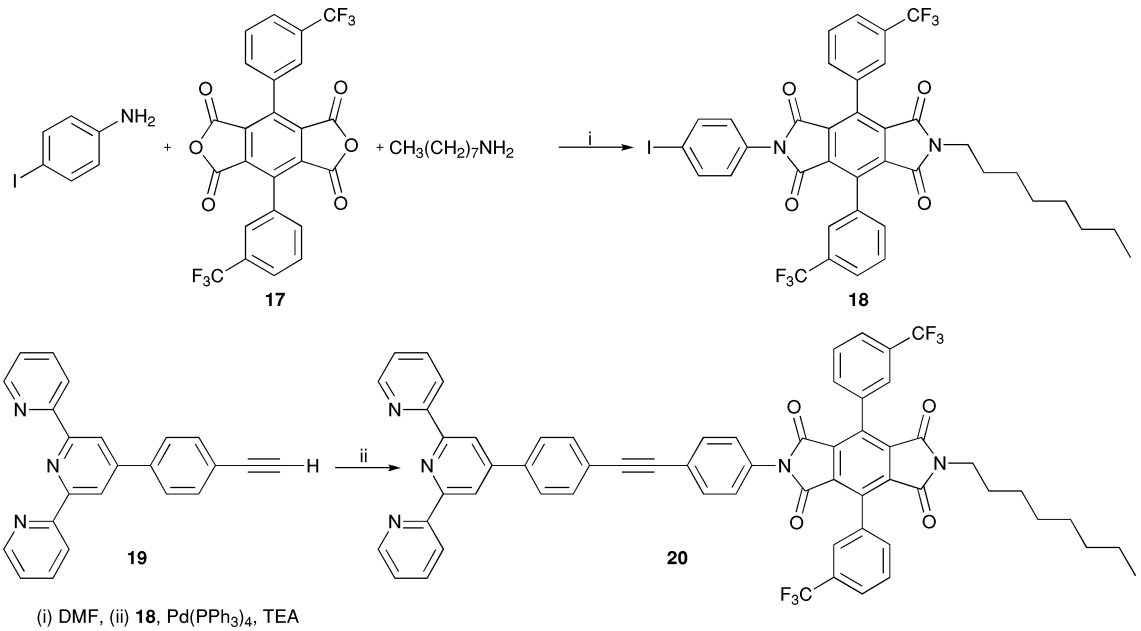

Scheme 3

Table 1 Summary of steady-state absorption data for **1–10**, $Ru(phtpy)_2^{2+}$ and $Os(phtpy)_2^{2+}$ in DMF

Compound	LC_{max} (nm) ($\varepsilon \times 10^4/M^{-1}$ cm^{-1})	$^1MLCT_{max}$ (nm) ($\varepsilon \times 10^4/M^{-1}$ cm^{-1})	$^3MLCT_{max}$ (nm) ($\varepsilon \times 10^4/M^{-1}$ cm^{-1})
$Ru(phtpy)_2^{2+}$	318 (6.16)	494 (2.35)	—
$Os(phtpy)_2^{2+}$	319 (6.05)	494 (2.55)	671 (0.72)
1	332 (6.35)	498 (3.36)	—
2	336 (7.32)	500 (3.53)	—
3	318 (7.76)	497 (3.09)	676 (0.82)
4	320 (7.85)	499 (3.17)	678 (0.89)
5	333 (6.42)	499 (3.13)	—
6	336 (7.56)	500 (3.74)	—
7	320 (7.88)	501 (3.21)	677 (0.79)
8	319 (7.98)	499 (3.40)	677 (0.77)
9	315 (6.79)	498 (1.65)	—
10	318 (7.37)	499 (1.62)	677 (0.23)

~3–7 nm from $Ru(phtpy)_2^{2+}$ and $Os(phtpy)_2^{2+}$. Similarly, the ^{3}MLCT bands in complexes **3–4** and **7–8** are red-shifted by ~5–7 nm from that of $Os(phtpy)_2^{2+}$. The shift to lower energy absorption bands most likely arises from the increase in conjugation of the metal terpyridine with the 4′-substituents.[27] The observed absorption spectra closely match the sum of the spectra for $Ru(phtpy)_2^{2+}$ or $Os(phtpy)_2^{2+}$ and DMB, BQ or PI, indicating little electronic interaction is present in the ground state complexes.

Electrochemistry

Cyclic voltammetry (CV) measurements were carried out on $Ru(phtpy)_2^{2+}$, $Os(phtpy)_2^{2+}$, and **1–10** in either DMF or CH_3CN and the results are summarized in Table 2. Interestingly, the E_{ox} values for the M^{3+}/M^{2+} couple in the Os-containing complexes varied little over all of the compounds studied. However, the analogous values for the Ru-containing compounds had a significant shift in potential as a function of substitution on the terpyridine ring, and varied from +0.782 to +0.836 V. In general, all DMB and quinone containing Ru-complexes were oxidized at more positive potentials than $Ru(phtpy)_2^{2+}$, while the pyromellitimide-containing complex was found to be slightly lower. The complexes containing two phenyl spacer groups (**2** and **6**) were found to have lower potentials than those with one phenyl spacer group (**1** and **5**), most likely as a result of the increased delocalization of charge. Electron transfer was calculated to be exergonic for quinone-containing complexes **5–8**, with free energies (ΔG_{ET}) in the range of –0.30 to –0.51 eV. Calculations using the reduction potentials of pyromellitimide-containing complexes **9** and **10** indicate replacement of the quinone group with the ethynylphenyl pyromellitimide group lowers the value of ΔG_{ET} so that they are barely exergonic (*i.e.*, –0.06 eV for **9** and –0.07 eV for **10**).

The electrochemical data presented here facilitated construction of the energy diagrams shown in Fig. 3, in which the energies of the ^{3}MLCT state are estimated in the usual manner from the wavelengths of the ^{3}MLCT emission.

Steady state emission

Steady state emission measurements were performed on both ruthenium(II) and osmium(II) complexes $Ru(phtpy)_2^{2+}$, $Os(phtpy)_2^{2+}$, and **1–10** at room temperature (Table 3). The emission spectra of the osmium(II) complexes are shown in Fig. 4. Similar to the results obtained in the steady-state absorption experiments, where the addition of each aryl group onto the metal terpyridine resulted in a red-shift in the absorption bands, a substitution dependent red-shift in the emission maxima of Ru-containing complexes **1–2** and **5–6** was observed. In the case of the Os-containing complexes **3–4** and **7–8**, the opposite trend was observed, and **3** and **7** have longer wavelength emission maxima than **4** and **8**. Åkermark, *et al.*[18] reported the quantum yield of $Ru(ttpy)_2^{2+}$ is too small to quantify reliably; we have found the same for $Ru(phtpy)_2^{2+}$, **1** and **2**, where the Φ_{em} values for **1** and **2** could not be accurately determined. Amongst the Os-containing standards, Φ_{em} for **4** was found to be lower by ~20% than that observed for either $Os(phtpy)_2^{2+}$

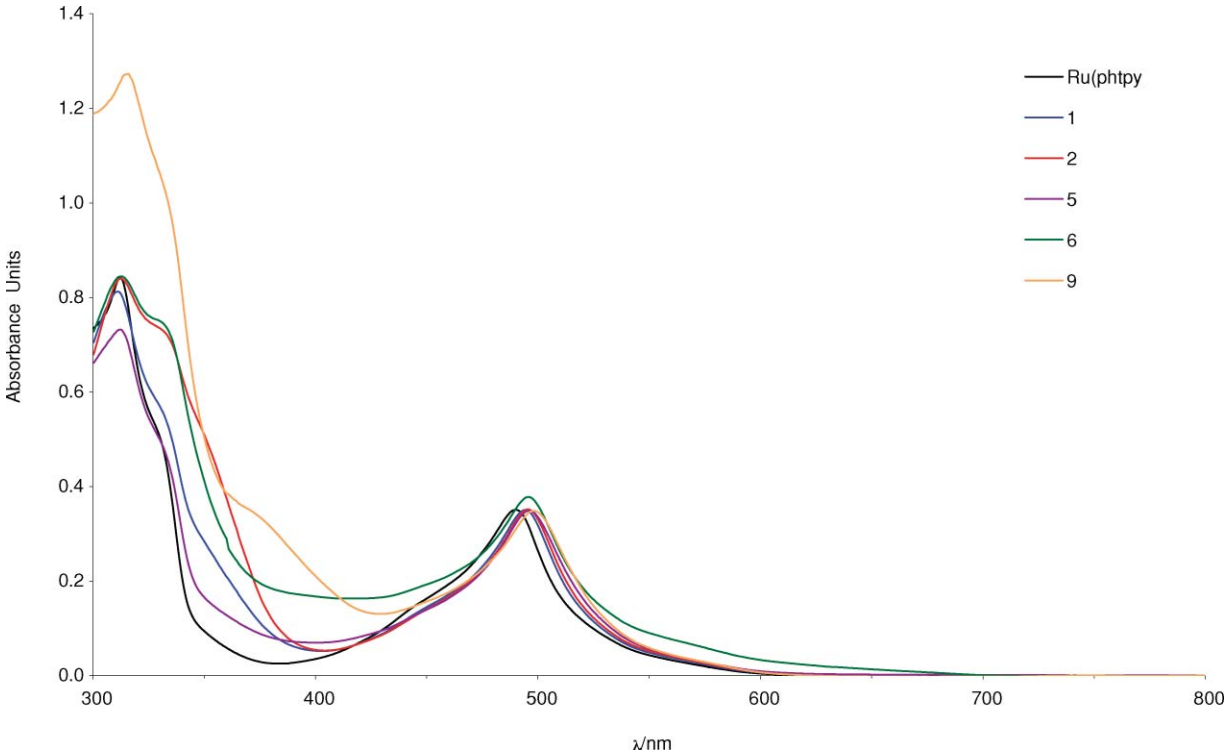

Fig. 1 Absorption spectra of Ru-containing terpyridine complexes $Ru(phtpy)_2^{2+}$, **1**, **2**, **5**, **6** and **9** in DMF.

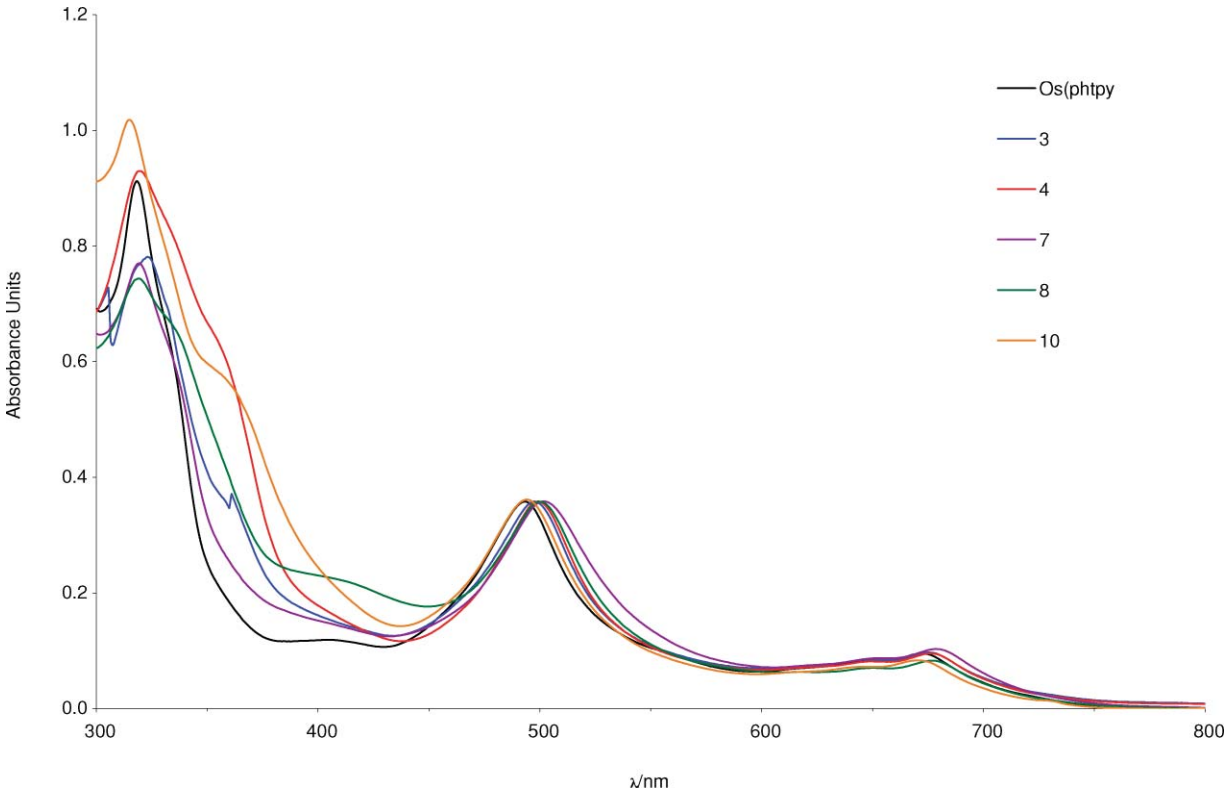

Fig. 2 Absorption spectra of Os-containing terpyridine complexes $Os(phtpy)_2^{2+}$, **3**, **4**, **7**, **8** and **10** in DMF.

Table 2 Electrochemical data for **1–10**, $Ru(phtpy)_2^{2+}$ and $Os(phtpy)_2^{2+}$[a]

Complex	$E_{1/2}$ (V) ($M^{3+/2+}$)	$E_{1/2}$ (V) ($M^{2+/+}$)	$E_{1/2}$ (V) ($M^{+/0}$)	$E_{1/2}$ (V) $(BQ)^{-/0}$ $(PI)^{-/0}$	E_{MLCT} (eV)	ΔG_{ET}[b](eV)
$Ru(phtpy)_2^{2+}$	0.802	—	−1.638	—	1.99	—
$Os(phtpy)_2^{2+}$	0.520	−1.583	−1.863	—	1.67	—
1	0.836	−1.400	−1.644	—	1.97	—
2	0.830	−1.424	−1.640	—	1.96	—
3	0.504	−1.585	−1.855	—	1.67	—
4	0.509	−1.562	−1.802	—	1.67	—
5	0.842	−1.488	−1.728	−0.800	1.94	−0.30
6	0.819	−1.581	−1.741	−0.810	1.96	−0.33
7	0.528	—	—	−0.773	1.68	−0.38
8	0.518	—	—	−0.647	1.67	−0.51
9	0.782	—	—	−1.18	2.02	−0.06
10	0.516	—	—	−1.15	1.74	−0.07

[a] Referenced to Fc^+/Fc, in either CH_3CN (Os-complexes) with 0.1 M $TBAPF_6$ as the supporting electrolyte or DMF (Ru-complexes) with 0.1 M TBAP as the supporting electrolyte, using platinum auxiliary and working electrodes. [b] Calculated using the equation: $\Delta G_{ET} = E_{1/2}(M^{3+/2+}) - E_{1/2}(A^{-/0}) - E_{MCLT}$, where A = BQ or PI.

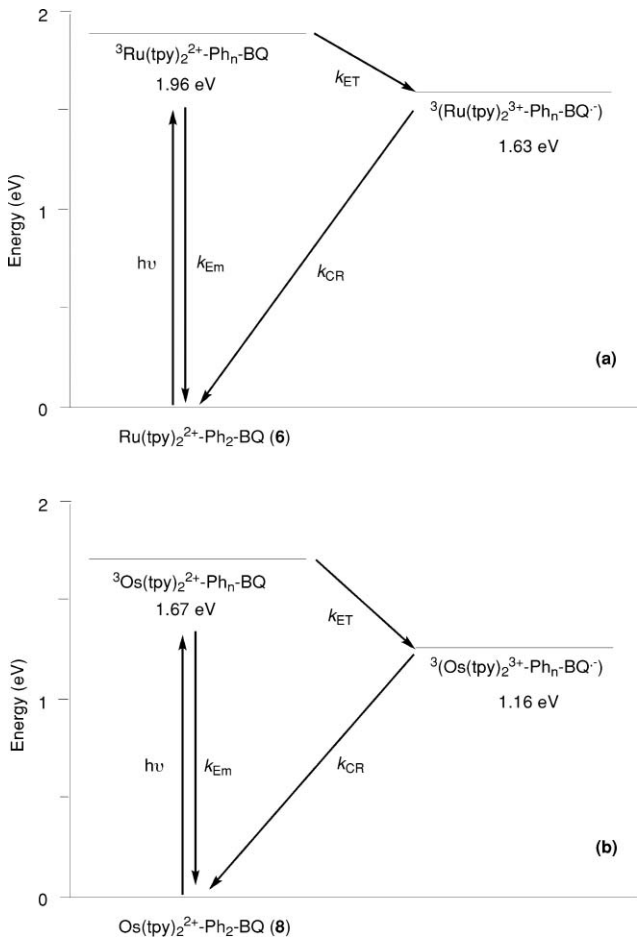

Fig. 3 Representative energy diagrams for quinone-containing dyads **6** (a) and **8** (b).

or **3**, the reason of which is unclear. The corresponding Φ_{em} values for the quinone-containing dyads **7–8** were reduced by two orders of magnitude relative to both $Os(phtpy)_2^{2+}$ and **3–4** (Table 3). Similarly, Φ_{em} for diimide-containing **10** is reduced from that of $Os(phtpy)_2^{2+}$ by ~35%. Because the only difference between the dimethoxybenzene-containing complexes (**3–4**) and the benzoquinone-containing (**7–8**) and PI-containing (**10**) complexes is replacement of the dimethoxybenzene groups with either benzoquinone or ethynylphenyl pyromellitimide groups, the decrease in the emission quantum yields **7–8** and **10** is attributed to intramolecular electron-transfer from the ^{3}MLCT-excited state of the osmium complex to the benzoquinone/PI acceptor group(s).

Table 3 Summary of steady-state and time-resolved emission data for $Os(phtpy)_2^{2+}$, $Ru(phtpy)_2^{2+}$ and **1–10**

Compound	Solvent	λ_{em} (nm)[a]	Φ_{em}[b–d]	τ (ns)[c]
$Os(phtpy)_2^{2+}$	CH_3CN	740	2.1×10^{-2}	232
$Ru(phtpy)_2^{2+}$	DMAc	629	—	—
1	DMAc	629	—	—
2	DMAc	640	—	—
3	CH_3CN	742	2.09×10^{-2}	219
4	CH_3CN	739	1.74×10^{-2}	215
5	DMAc	642	—	—
6	DMAc	645	—	—
7	CH_3CN	744	1.79×10^{-4}	—
8	CH_3CN	742	2.56×10^{-4}	—
9	DMAc	648	—	—
10	DMF	747	7.30×10^{-3}	168

[a] Values were recorded at 25°C in argon saturated solutions with excitation at 500 nm. [b] Assuming the value for $Os(phtpy)_2^{2+}$ is similar to that of $Os(ttpy)_2^{2+}$ ($\Phi_{em} = 2.1 \times 10^{-2}$)[7]. [c] Values for the Ru(II) complexes could not be obtained because of their weak emission. [d] Experimental values are all reported with error limits of ±10%.

The emission quantum yield data indicates electron-transfer is slightly more efficient in **7** than **8**. The exponential dependence of k_{ET} on the donor–acceptor distance is well known,[28] and it is therefore not surprising that the emission quantum yield of **8**, containing two phenyl spacer groups, is ~30% larger ($\Phi_{em} = 2.56 \times 10^{-4}$) than that of **7**, which contains only one phenyl spacer (Φ_{em} ~1.79×10^{-4}). When the bias from the substitution patterns on the model compounds is considered using relative emission quantum yields (*i.e.*, Φ_7/Φ_3 and Φ_8/Φ_4),[29] the relative difference (~43%) between the two dyads is greater still, and Φ_7/Φ_3 ~8.6×10^{-3} and Φ_8/Φ_4 ~1.5×10^{-2}. However, these values are nonetheless quite small and indicate electron-transfer is the major photophysical process consuming the excited states of both **7** and **8**. Thus, when the electron-transfer efficiency is considered (eqn (1), where ϕ_{ET} is the electron-transfer efficiency, Φ_{DA} is the quantum yield of the donor–acceptor dyad and Φ_D represents the quantum yield of the

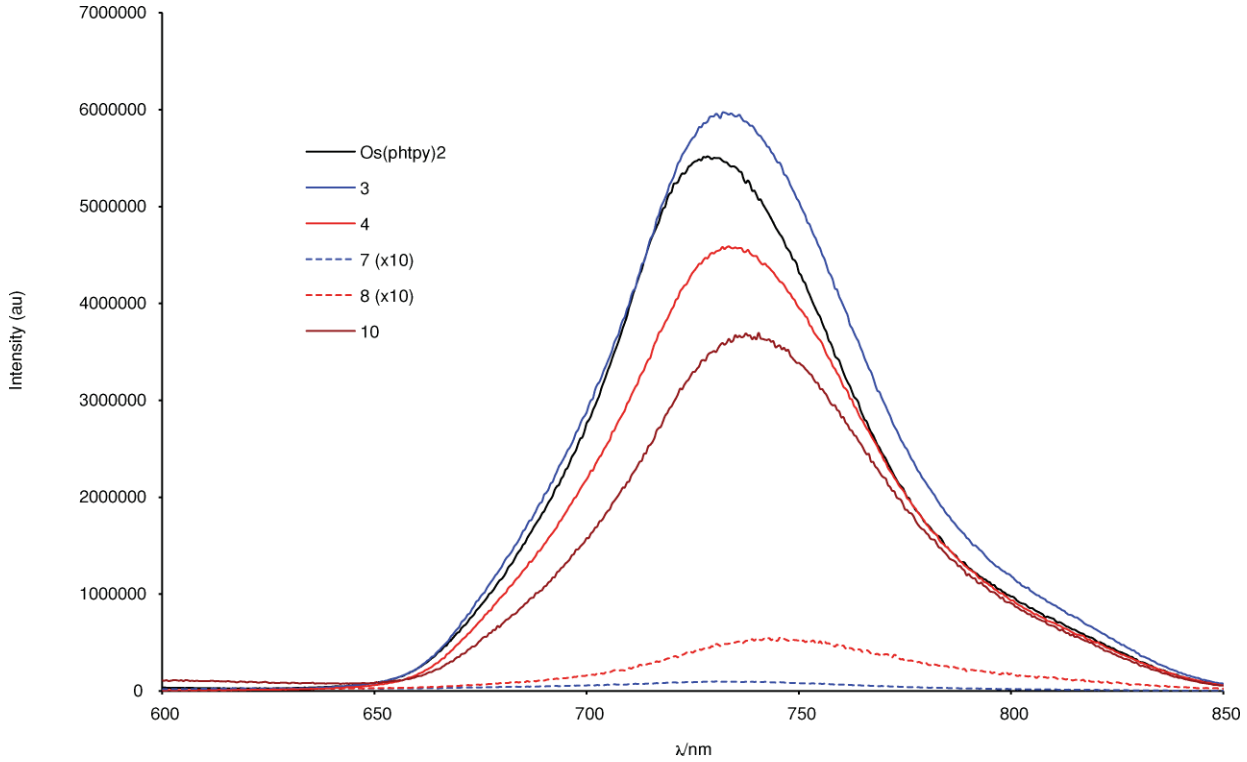

Fig. 4 Steady-state emission spectra measured for $Os(phtpy)_2^{2+}$, model compounds **3–4**, and dyads **7–8**.

donor), the amount of electron-transfer in these compounds is found to be near unity (99.1 for **7** and 98.5% for **8**)

$$\phi_{ET} = 1 - \Phi_{DA}/\Phi_{D} \quad (1)$$

Thus, while the addition of the extra phenyl spacer in **8** may play an important role in slowing ET, the overall efficiency in both dyads is nonetheless quite high. The quantum yield of emission for **10** was found to be 7.30×10^{-3}, with ϕ_{ET} ~65%. The greater amount of emission (and lower yield of electron-transfer) in this compound is consistent with the significantly smaller driving force for ET in this dyad (ΔG_{ET} ~ –0.07 eV) compared to **7** (–0.38 eV) or **8** (–0.51 eV).[30]

Time-resolved emission

Emission lifetimes (τ_{em}, Table 3) were determined for Os-containing complexes $Os(phtpy)_2^{2+}$, **3**, **4** and **10** by exciting the samples with the 565 nm, ~6 ns, pulses of a Nd:YAG pumped dye laser and monitoring the decay profiles at 740 nm. These compounds all exhibited monoexponential decays. The emission lifetimes of **3–4** (219 and 215 ns, respectively) were found to be similar to that of $Os(phtpy)_2^{2+}$ (τ_{em} ~232 ns),[5] while the emission lifetime of **10** was determined to be ~168 ns. Determination of the emission lifetimes for quinone-containing complexes **7** and **8** was attempted using time-correlated single-photon counting (TC-SPC) experiments with picosecond excitation. The low emission quantum yields of these complexes made the determination of τ_{em} for these compounds impossible with any accuracy. Similarly, the emission lifetimes of any of the ruthenium-containing compounds could not be quantified because of their very low emission quantum yields.

Time-resolved absorption

A combination of femtosecond and nanosecond transient absorption and time-resolved spectroscopy was used to investigate the excited state lifetimes of model compounds **1–4** and to determine the electron-transfer (k_{ET}) and charge-recombination (k_{CR}) rate constants in dyads **5–10** (Table 4). Excitation of ~3×10^{-6} M acetonitrile or DMAc solutions of **1–4** with ~130 fs, 500 nm laser pulses resulted in the appearance of the transient absorption spectra corresponding to the ^{3}MLCT states of the respective $Ru(phtpy)_2^{2+}$ and $Os(phtpy)_2^{2+}$ groups. The spectrum of $Ru(phtpy)_2^{2+}$ in DMAc at a time delay of 1 ns is characterized by a sharp absorption band at ~400–420 nm, a single broad absorption centered at ~590 nm, and a bleach of the ground state absorption at ~500 nm. The transient absorption spectra of dimethoxybenzene-substituted model compounds **1** and **2** at similar time delays are similar to that of $Ru(phtpy)_2^{2+}$, and have intense absorptions at ~400–420 nm and weaker and very broad absorptions centered at ~610 nm (**1**) and ~635 nm (**2**), respectively, as well as the ground state bleach at ~500 nm. The red-shifted excited state absorption band for **2** is consistent with the red-shifts observed in the ground state absorption spectrum of this compound. The time-dependent data on the sub-picosecond time-scale are characterized by an ultrafast growth in absorption in the high-energy region of the transient absorption spectrum (~400–450 nm) that is followed by an equally rapid decay. Both of these processes are pulse-width limited (<200 fs) and probably result from the initial growth of the ^{1}MCLT state followed by intersystem crossing to the ^{3}MLCT state. The rise-time of the low energy transient absorption band at ~600 nm associated with the ^{3}MLCT state is on the same time-scale as the rapid decay in the 400 nm region of the spectrum, providing

Table 4 Summary of transient and time-resolved absorption data for $Ru(phtpy)_2^{2+}$, $Os(phtpy)_2^{2+}$ and **1–10**

Compound	Solvent	$\lambda_{LC}/\lambda_{BQ^-}$ (nm)	τ_{BQ}	λ_{bleach} (nm)	τ_{bleach}	λ_{MLCT} (nm)	τ_{MLCT}	k_{ET} (s^{-1})	k_{CR} (s^{-1})
$Ru(phtpy)_2^{2+}$	DMAc	400		490	1.28 ns	591	1.28 ns		
$Os(phtpy)_2^{2+}$	CH_3CN	400		490		590	232 ± 12 ns		
1	DMAc	400		500		610	1.35 ± 0.10 ns		
2	DMAc	400		500		635	1.78 ± 0.10 ns		
3	CH_3CN	390		500		590	219 ± 11 ns		
4	CH_3CN	400		500		590	218 ± 11 ns		
5	DMAc	410		515	47 ± 6.0 ps	600	13 ± 1.4 ps	$7.6 \pm 0.8 \times 10^{10}$,[c]	$2.1 \pm 0.3 \times 10^{10}$,[d]
6	DMAc	410		515	19 ± 2.3 ps	600	43 ± 0.1 ps	$2.3 \pm 0.1 \times 10^{10}$,[c]	$5.3 \pm 0.6 \times 10^{10}$,[d]
7	DMAc	430	4.0 ± 0.8 ps[a] 16 ± 0.5 ps[b]	520	14 ± 1.4 ps	~600	6.7 ± 0.2 ps	$1.5 \pm 0.1 \times 10^{11}$,[c] $2.5 \pm 0.2 \times 10^{11}$,[e]	$6.3 \pm 0.1 \times 10^{10}$,[d] $7.1 \pm 0.8 \times 10^{10}$,[d]
8	DMAc	430	—[g] 86 ± 0.5 ps[b]	520	84 ± 0.2 ps	600	75 ± 0.5 ps	$1.3 \pm 0.1 \times 10^{10}$,[c] —[e,g]	$1.2 \pm 0.1 \times 10^{10}$,[d] $1.2 \pm 0.1 \times 10^{10}$,[f]
9	DMAc	415		515		600	6.1 ± 0.9 ns		
10	DMAc	420		495	130 ± 13 ns	433 580	116 ± 11 ns	$4.3 \pm 0.1 \times 10^6$	$7.7 \pm 0.1 \times 10^6$

[a] The time constant for the growth at this wavelength. [b] The time constant for the decay at this wavelength. [c] The electron-transfer rate constant calculated using the decay at 600 nm. [d] The charge-recombination rate constant calculated using the recovery of the bleach at 520 nm. [e] The electron-transfer rate constant calculated using the growth at 430 nm. [f] The charge-recombination rate constant calculated using the decay at 430 nm. [g] Unable to determine.

further evidence for this process. Similar rapid decay/growth kinetics have been reported for $Ru(bpy)_3^{2+}$ and $Os(bpy)_3^{2+}$ by Durant[31] and McKusker.[32,33]

On the nanosecond time-scale, the time-dependent decays in these spectral regions are monoexponential for all three Ru-containing model compounds (1.28–1.78 ns, Table 4). Examination of the absorption spectra of dyads **5**–**6** and **9** show similar spectral features to those of the model compounds ($Ru(phtpy)_2^{2+}$, **1** and **2**), with a strong sharp absorption band centered around 410–420 nm, a weaker shoulder at ~430–440 nm and a very broad absorption centered in the 600–660 nm range. The 500 nm bleach of the ground state absorption was observed in all dyads. The spectrum of **6** taken at different delay times is shown in Fig. 5.[34] The kinetic profiles of dyads **5**–**6** recorded both at the absorption and bleach wavelengths indicate a significant decrease in the absorption intensities of the bands at ~410 (λ_{410}) and ~600 nm (λ_{600}) as a function of time, as well as a recovery of the ground state bleach at ~515 nm (λ_{bleach}). The decay at 600 nm and the bleach at 515 nm were fit to single exponential functions, with lifetimes of τ_{600} ~13 ps (600 nm) and τ_{bleach} ~47 ps (515 nm) for the absorption and bleach bands of **5**, and τ_{600} ~43 ps and τ_{bleach} ~19 ps for these bands in **6**. Both sets of lifetimes are significantly shorter than the lifetimes of the analogous bands in the model compounds. Harriman and co-workers[35] have recently shown the decay of the 600 nm ^{3}MLCT band can be used to monitor electron transfer in a Ru(tpy)-Q dyad, although their work also showed the lifetimes of both the bleach and the ^{3}MLCT bands to be the same. Spectroelectrochemical measurements by Brewer and coworkers on various $Ru(tpy)(tpp)^{2+}$ (where tpp is 2,3,5,6-tetrakis(2-pyridyl)pyrazine)[36] and $Os(tpy)(tpp)^{2+}$ complexes[37] indicates a bleach occurs in the ^{3}MLCT region (at ~500 nm) upon one-electron oxidation of the complex, and recovery of this band is consistent with charge-recombination and regeneration of the ground state. We therefore attribute the 600 nm absorption to represent electron transfer, while the recovery of the bleach band represents repopulation of the ground state, and therefore charge recombination. From this data, we calculate k_{ET} ~7.6×10^{10} s^{-1} for **5** and k_{ET} ~2.3×10^{10} s^{-1} for **6**, while charge recombination is found to occur in k_{CR} ~2.1×10^{10} s^{-1} and k_{CR} ~5.3×10^{10} s^{-1}, for **5** and **6**, respectively.

The femtosecond time-resolved absorption spectrum of $Os(phtpy)_2^{2+}$ at a time delay of 1 ns is characterized by broad absorption bands centered at 400 and 590 nm, and ground state depletion bands at ~490 and 670 nm. The femtosecond transient absorption spectrum of **3** at a similar time delay shows a low energy absorption band at ~580 nm and a higher energy absorption band at ~390 nm, while the transient absorption spectrum of complex **4** shows a slightly red-shifted low energy band at 590 nm as well as the high energy band at ~390 nm. All transient absorption spectra show large ground state bleaches at ~500 nm. The temporal evolution of the absorption bands, together with the recovery of the ground state bleach, were measured in time-resolved experiments on both the femtosecond and nanosecond time-scales with probe wavelengths corresponding to the absorption spectra peak maxima. Time-resolved spectra taken at short-times (*i.e.*, 0–20 ps) for model compounds $Os(phtpy)_2^{2+}$ and **3**–**4** display a pulse-width limited growth at ~400 nm, followed by an ultrashort decay, that in turn is followed by a second ultrashort growth having the same time constant as the ultrafast decay. These processes occur on a time-scale faster than the time-resolution of our instrument (*i.e.*, < 200 fs), similar to that observed for the analogous Ru-containing compounds,[31,32] and likely resulting from the rapid decay of the initially formed ^{1}MLCT state followed by the concomitant growth of the ^{3}MLCT state. The ^{3}MLCT state does not decay on the time-scale of these experiments, and the kinetic profiles for **3**–**4** were therefore obtained using nanosecond time-resolved experiments. The lifetimes of these compounds were found to be 232 ns for $Os(phtpy)_2^{2+}$, and 219 ns and 218 ns for **3** and **4**, respectively (Table 4). These values are similar to those obtained by time-resolved emission (Table 3) and reported previously[7a] for $Os(phtpy)_2^{2+}$, and indicate substitution only mildly affects the lifetimes of **3** and **4**.

The transient absorption spectra of dyads **7**–**8** taken at early times (<10 ps) are similar to those of the respective model compounds **3** and **4** (λ_{600} ~600 nm and λ_{bleach} ~500 nm), but also show a pronounced shoulder at ~430 nm (λ_{430}). Fitting of the

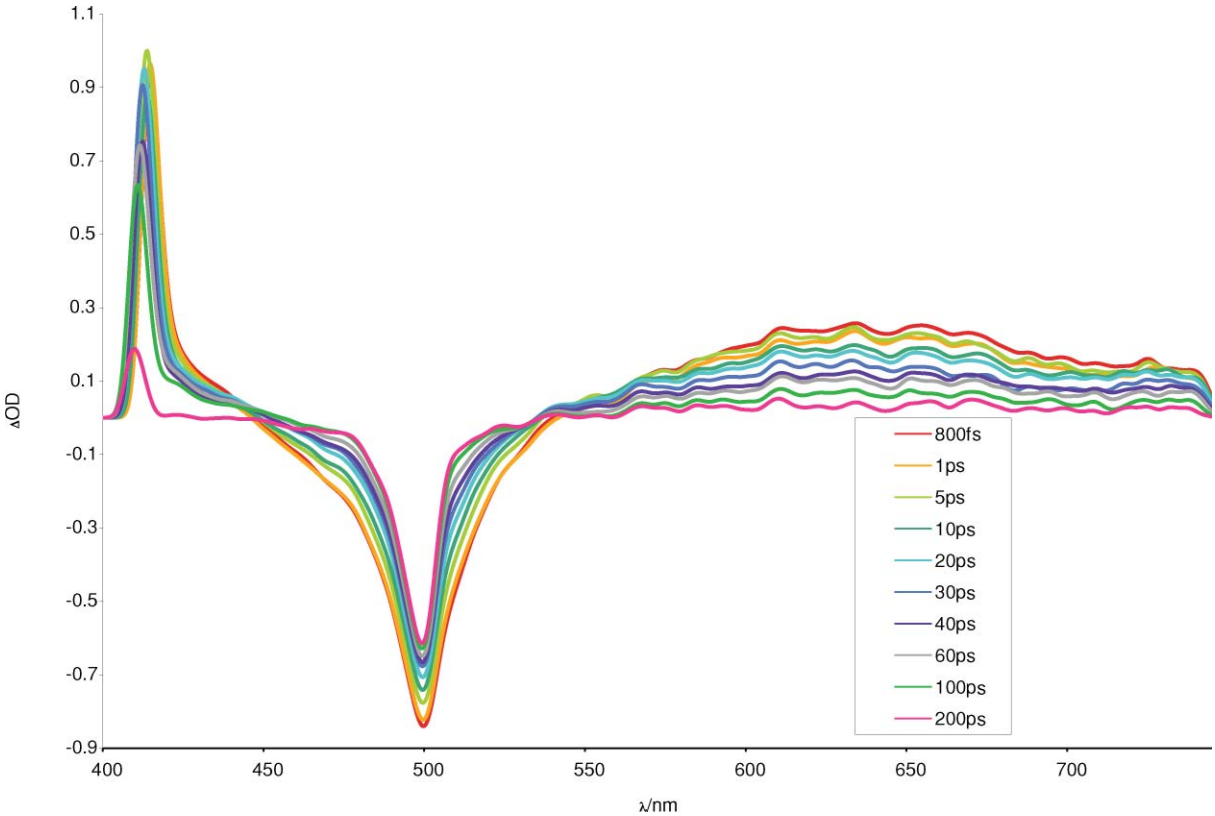

Fig. 5 A series of representative transient absorption spectra are shown for **7** in acetonitrile as a function of time.

time-resolved traces at the 400 and 600 nm transient absorption bands displays the ultrafast decay/growth kinetics described earlier. At slightly longer delay times, a marked decrease was observed in all three bands (shown for **7**, Fig. 6).[38] Because of the pronounced shoulder at 430 nm in the spectra of **7** and **8**, the growth of this band was also fit in the time-resolved spectra of **7** and **8**. Time-resolved absorption measurements for the 430 nm transient absorption band of **7** displayed a monoexponential growth of τ_{430} ~4.0 ps, followed by a decay of τ_{430} ~16 ps, while the band at 600 nm had a monoexponential decay of τ_{600} ~6.7 ps. The bleach recovery, measured at the red-edge of the depletion at 520 nm, had a monoexponential decay of τ_{bleach} ~14 ps. In the case of dyad **8**, we were unable to fit the growth of the band at 430 nm to a χ^2 value lower than 1.4, possibly because the absorption overlapped too strongly with the more intense band centered at 420 nm. We were able to fit the decay at 430 nm in **8**, however, which was found to be monoexponential (τ_{430} ~86 ps) as was the decay at 600 nm (τ_{600} ~75 ps) and the recovery of the bleach at 520 nm (τ_{bleach} ~84 ps). The growth and decay of the absorption band at ~430 nm band in both **7** and **8** is attributed to the reduction and subsequent reformation of benzoquinone.[39] In the case of **7**, the rise of this band (~4.0 ps) corresponds within experimental error with the decay at 600 nm (~6.7 ps), and is consistent with the assignment of charge separation to the decay value of the ^{3}MLCT band. Importantly, the decay at 430 nm (~16 ps) corresponds very well with the recovery of the ground state bleach at ~520 nm (~14 ps), consistent with charge recombination. Similarly, the lifetimes of the decay at 430 nm and the bleach recovery at 520 nm in **8** are nearly the same, within experimental error. Taking the decay of the 600 nm ^{3}MLCT band to arise from charge separation, and the 520 nm bleach to represent charge-recombination, we calculated the ET and CR rate constants for **7** (k_{ET} ~1.5–2.5 × 10^{11} s^{-1}—by following the 600 nm and 430 nm bands, respectively, and k_{CR} ~6.3–7.1 × 10^{10} s^{-1}–by following the 520 nm and 430 nm bands, respectively) and **8** (k_{ET} ~1.2 × 10^{10} s^{-1} and k_{CR} ~1.2 × 10^{10} s^{-1}).

The transient absorption spectra of diimide-containing complexes **9–10** were found to be similar to those of **5–8**, but decayed on significantly slower time-scales. The time-dependent transient absorption results for **9** at 600 nm at short times (*i.e.*, 0–10 ps) indicate a fast growth component of < 200 fs, similar to what was observed in the other metal-terpyridine complexes and is again attributed to formation of the ^{3}MLCT state. At longer times (0–8 ns), **9** shows a relatively long-lived monoexponential decay of τ_{600} ~6.1 ns that is slightly longer than the lifetime of the diethynyl-substituted $Ru(phtpy)_2^{2+}$ model compound ruthenium 4′-ethynylphenylterpyridine ($Ru(phactpy)_2^{2+}$, for which τ_{600} ~5.0 ns. The similarities in the lifetimes between **9** and the model compounds $Ru(phactpy)_2^{2+}$, $Ru(tpy)_2^{2+}$, **1** and **2**, indicates electron transfer is not an important pathway in the decay of dyad **9**. Given the relatively low free energy for electron transfer (ΔG_{ET} −0.06 eV) and the short ^{3}MCLT lifetime of the parent molecule, the lack of charge separation in this complex is not surprising. Hammarström and co-workers have recently reported[18,40] electron transfer in a similar Ru(II)-PI, although in this dyad the PI group was directly attached *via* a methylene linking group to the terpyridine, and not through an ethynlphenyl terpyridine linker. We assume that the shorter D–A distance in this compound makes ET more favorable.

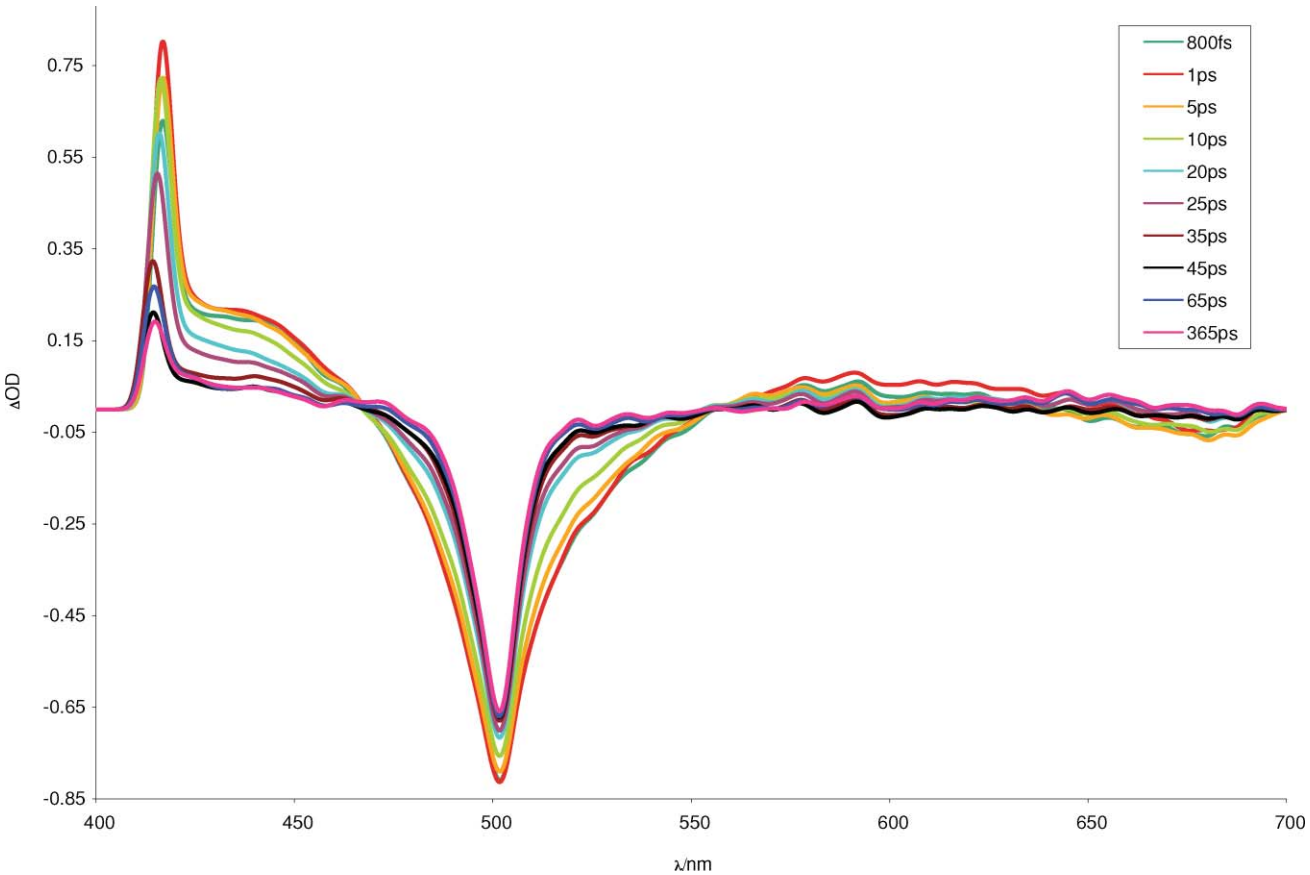

Fig. 6 A series of representative transient absorption spectra are shown for **7** in acetonitrile as a function of time.

Unlike **9**, diimide **10** apparently does undergo charge separation. Nanosecond-resolved transient absorption experiments on **10** in DMAc yielded a transient absorption spectrum similar to the other Os-containing complexes, with a bleach at ~495 nm and the ^{3}MLCT absorption band at ~590 nm. Conspicuously absent from this spectrum was the absorption band at 430 nm that we have attributed to the benzoquinone radical anion in **7** and **8**. The absorption at 590 nm, attributed to charge separation in **7** and **8**, was found to decay with τ_{590} ~116 ns, while the ground state bleach at 495 nm was found to recover with τ_{bleach} ~130 ns. Unfortunately, the characteristic absorption feature typically observed for the pyromellitimide radical anion at ~715 nm[41] was not observed because of the strong overlapping absorption from the $Os(phtpy)_2^{2+}$ ^{3}MLCT state. From the time-resolved luminescence data we reported a lifetime for the ^{3}MLCT band of ~168 ns, on the same order of magnitude as the decay of the ^{3}MLCT in the nanosecond transient absorption experiments. From this data it appears electron-transfer in **7** occurs with charge separation rate constants of k_{ET} ~4.3×10^6 s^{-1}, whereas charge recombination occurs with a faster rate constant of k_{CR} ~7.7×10^6 s^{-1}.

Discussion

Because the transient absorption spectra of the ^{3}MLCT states in both $Os(phtpy)_2^{2+}$ and $Ru(phtpy)_2^{2+}$ are quite similar to those of the corresponding oxidized metal bisterpyridines, meaningful differentiation between the absorption bands in the transient absorption spectra is difficult. Nonetheless, careful examination of the time-dependent absorption spectra of **5–8**, and **9–10** reveals useful information. In both the Ru and Os-containing dyads, the absorption (~600–635 nm) and bleach recovery (500 nm) bands in the transient absorption spectra yield different time constants, indicating these bands represent two different photophysical processes. An additional band at 430 nm was observed for **7** and **8**, for which the decay constant correlates with the recovery of the ground state bleach band at 520 nm. For **7**, the growth of the 430 nm band was resolved, and for this reason we first interpret the photophysical events occurring upon electronic excitation of dyad **7**. The radical anion of benzoquinone ($BQ^{\bullet -}$) is known to have an absorption band at ~425–445 nm,[39] similar to the band observed in dyad **7** at 430–440 nm. This band provides us with an independent set of rate constants with which to evaluate the absorptions in the rest of the transient absorption spectra. The band at 600 nm clearly corresponds to the ^{3}MLCT absorption, and its disappearance correlates with decay of the ^{3}MLCT state and therefore electron-transfer. The bleach at 500 nm is actually a superposition of two bands, the first of which corresponds to ground state depletion. The second band is known, from the spectroelectrochemistry of $Ru(phtpy)_2^{2+}$, to correspond to a bleach in the difference spectrum of $Ru(tpy)_2^{2+}/Ru(tpy)_2^{3+}$.[36] Assuming $Ru(phtpy)_2^{3+}$ is spectroscopically similar to that of $Os(phtpy)_2^{3+}$, we can then fully interpret the time-resolved data. By resolving the growth and decay of the 430 nm band in the femtosecond transient absorption experiments, we are able to attribute the growth at

this wavelength to the formation of the BQ radical anion, and its decay the result of charge-recombination. The value fitted for the decay of the ^{3}MLCT band at 600 nm (τ_{600} ~6.7 ps) is close to the 4.0 ps growth observed at 430 nm ($k_{ET} \sim k_{430}$ ~2.5×10^{11} s^{-1}), and the ^{3}MLCT decay is (as expected) therefore assigned to charge-separation ($k_{ET} \sim k_{600}$ ~1.5×10^{11} s^{-1}).[35] The time-constant (τ_{bleach} ~14 ps) for the recovery of the ground state bleach (measured at 520 nm) matches the decay at 430 nm (τ_{430} ~16 ps, $k_{CR} \sim k_{430}$ ~7.1×10^{10} s^{-1}), and therefore the recovery of the bleach signal is also assigned to charge-recombination ($k_{CR} \sim k_{600}$ ~6.3×10^{10} s^{-1}). With this analysis in mind, we can dissect the rate constants of dyads **5–6** and **8**.

In all cases, the decay of the ^{3}MLCT state absorption band at 610–635 nm in **5–8** results from electron-transfer (Ru(II)-BQ → Ru(III)-BQ$^-$ and Os(II)-BQ → Os(III)-BQ$^-$), consistent with the assignment of Benniston *et al.*,[35] while the recovery of the ground state bleach measured at 520 nm is assigned to charge recombination of the charge separated pairs (Ru(III)-BQ$^-$ → Ru(II)-BQ and Os(III)-BQ$^-$ → Os(II)-BQ). For **5**, the rate constants for these bands correspond to $k_{ET} \sim k_{600}$ ~7.6×10^{10} s^{-1} for charge separation and $k_{CR} \sim k_{bleach}$ ~2.1×10^{10} s^{-1} for charge recombination (Table 4), and for **6** the values are $k_{ET} \sim k_{600}$ ~2.3×10^{10} s^{-1} for charge separation and $k_{CR} \sim k_{bleach}$ ~5.3×10^{10} s^{-1} for charge recombination. In the case of Os-containing **8**, where the 430 nm absorption growth could not be resolved satisfactorily, the rate constants for the decay of the 430 nm absorption $k_{CR} \sim k_{430}$ ~1.2×10^{10} s^{-1} and 520 nm ground state bleach recovery $k_{CR} \sim k_{bleach}$ ~1.2×10^{10} s^{-1} are identical and correspond to charge recombination. Charge separation was monitored at the ^{3}MLCT band (600 nm) and was found to occur with a rate constant of $k_{ET} \sim k_{600}$ ~1.3×10^{10} s^{-1}.

At this point it is worthwhile to compare the results for the six dyads. In the Ru-containing dyad **5**, charge separation (k_{ET} ~7.6×10^{10} s^{-1}) is faster than charge recombination, which occurs with a rate constant of k_{CR} ~2.1×10^{10} s^{-1}, while the opposite is observed for dyad **6** where charge separation occurs with a rate constant of $k_{ET} \sim 2.3 \times 10^{10}$ s^{-1} and charge recombination with a rate constant of $k_{CR} \sim 5.3 \times 10^{10}$ s^{-1}. In order to address this switch in k_{ET} and k_{CR}, it is helpful to first consider the structures of biphenyl, 4-phenylpyridine (and its derivatives) and 4,4′-diphenylbipyridine in the ground and excited states. The ground state structure of biphenyl has a dihedral angle of 15–30° (in solution)[42] to 45° (gas phase)[43] between the phenyl rings, while excitation into its S_1 excited state twists the phenyl rings to be nearly co-planar (~0°) with one another.[44] Calculations on both 4-phenylpyridine and 4,4′-diphenylbipyridine indicate similar structural changes upon both one-electron reduction and electronic excitation of the ground state molecule.[45] We speculate such a structural change also occurs upon excitation of Ru(phtpy)$_2^{2+}$. Calculations[46] and experiments[47] have both indicated that bridge orientation plays an important role in determining the strength of the electronic coupling matrix and the resulting electron-transfer rate constant between porphyrins in aryl-linked diporphyrin dyads, with more planar orientations leading to more rapid electron-transfer. According to this mechanism, excitation of the Ru(phtpy)$_2^{2+}$ group in **5** would result in the bridging phenyl group becoming co-planar with the central terpyridine ring and the quinone, increasing the electronic coupling matrix between these two groups and thereby increasing k_{ET} relative to the case when the phenyl group does not rotate. Subsequent rotation of the phenyl group back to its original orientation within the charge-separated state removes the favorable electronic coupling and slows charge recombination in this dyad. For dyad **6**, the addition of the second phenyl group between the Ru(phtpy)$_2^{2+}$ and the quinone groups acts to insulate the Ru(tpy)$_2^{2+}$ and benzoquinone groups from one another, and the resulting rotation does not affect the coupling matrix in the same way. Similar results are observed for the Os-containing dyads **7** and **8**. In the case of **7**, the electron-transfer rate constant is more rapid than charge recombination by a factor of approximately three, while the electron-transfer and charge recombination rate constants for **8** are nearly identical. Again, presumably the Os(phtpy)$_2^{2+}$ excited state in **7** undergoes phenyl group rotation leading to an enhancement of the electronic coupling.[48]

In terms of the pyromellitimide-containing dyads, we note that charge separation in **10** is a relatively efficient process (~65% according to the emission quantum yield), whereas we observe no evidence for charge separation in dyad **9**. In all likelihood, this difference is a result of the much longer ^{3}MLCT state lifetime of the parent compound (~230 ns for Os(phtpy)$_2^{2+}$ compared to ~1.5 ns for Ru(phtpy)$_2^{2+}$ and ~5.0 ns for Ru(phactpy)$_2^{2+}$) that allows for electron transfer to compete with non-radiative decay channels. The charge separation rate constant is several orders of magnitude slower than the corresponding quinone-containing dyads, and is likely a result of the significantly smaller free energy for electron transfer than is found in the dyads containing the quinone acceptor, and a larger D–A distance than similar complexes observed by other groups.[18,40]

Experimental

General methods

All reactions were run under a nitrogen atmosphere unless indicated otherwise. THF was distilled from the Na/benzophenone ketyl and CH_2Cl_2 was distilled from CaH_2; all other solvents were used as received. All starting materials were used as received from Aldrich, Acros or Lancaster Synthesis. Flash chromatography was carried out on silica gel (230–400 mesh) or neutral alumina (60–325 mesh). All melting points were taken using a Thomas-Hoover capillary melting point apparatus and are uncorrected. Proton (^{1}H, 300 MHz) and proton-decoupled carbon (^{13}C, 75 MHz) NMR spectra were acquired using a Varian Gemini 300 MHz NMR. ESI-MS spectra were acquired with a Bruker (Billerica, MA) Esquire-LC electrospray ionization quadrupole ion trap mass spectrometer (ESI-QIT-MS). Samples were prepared by dissolving the solid samples at 10^{-4} M in CH_3CN, and were directly infused into the mass spectrometer at a flow rate between 100–300 μL h^{-1}. The ESI was operated with a capillary offset of 65–85 V, and a skimmer potential of 20–57 V. Ions were observed in both the +1 and +2 charge states, as $[M]^{2+}$, $[M + PF_6]^+$, and $[M + OH]^+$, and occasionally as $[M - H]^+$.

Absorption spectra were recorded on a Shimadzu Model UV-1601 spectrophotometer. Steady-state emission measurements were run on an ISA Jobin Yvon-SPEX Fluorolog 3–22 fluorometer having dual input and output monochromators. Emission spectra were collected using argon-saturated solutions by exciting at the MLCT maxima in S/R mode to correct for changes in the lamp

output intensity. Emission spectra were also corrected for grating and detector response. Quantum yield measurements were made relative to $Os(ttpy)_2^{2+}$ ($\Phi_{em} = 2.1 \times 10^{-2}$) and are reported with error limits of ±10%.[5]

Time-resolved emission measurements

All solvents used for spectroscopic measurements were either Spectral or HPLC-grade. Time-resolved emission experiments were performed in the picosecond time domain using the time-correlated single-photon counting (TCSPC) technique, and in the nanosecond regime by collecting the emission using a monochromator-photomultiplier setup. The experimental apparatus used in the former case utilizes the pulses from a Coherent 702 dye laser pumped by the 527 nm output of a mode-locked Nd:LYF laser. Emission signals in this system are detected at 54.7° with an emission polarizer and depolarizer using a Hamamatsu R3809U-51 red-sensitive multichannel plate detector. Data collection and analysis were accomplished with an Edinburgh Instruments data collection system and Pico-Quant FluoFit software, respectively. The time-resolution of this system is estimated at ~10 ps after reconvolution. In nanosecond experiments, the osmium complexes were excited with the 565 nm output of a Lambda Physik Scanmate 2E dye laser pumped by a Spectra Physics PRO-190 Nd:YAG laser. The emission was collected at a right angle to the excitation beam and collimated into a monochromator and a Hamamatsu R5108 photomultiplier tube. The data from the PMT was collected with a digitizing oscilloscope, transferred to a PC and analyzed. All experiments were run under an argon atmosphere. Most measurements were fit such that values of χ^2 between 0.9–1.20 were obtained. Error limits in these measurements are typically ±10%.

Electron–transfer rate constants determined from the time-resolved emission experiments were calculated using eqn (2):

$$k_{ET} = \frac{1}{\tau_{DA}} - \frac{1}{\tau_{D}} \quad (2)$$

where τ_{DA} represents the excited state lifetime of the benzoquinone- and diimide-containing complexes and τ_D represents the excited state lifetime of the reference compound.

Femtosecond pump–probe experiments

All solvents used for spectroscopic measurements were either Spectral or HPLC-grade. Time-resolved absorption experiments were performed using a regenerative and multipass amplifier mode-locked fs/ps Ti:sapphire pumped by a Q-switched and frequency doubled Nd:YLF laser, and in turn seeded by a Ti:sapphire laser. The laser pulses generated had an average temporal width of 130 fs at 800 nm and a repetition frequency of 1 kHz. The output was split and passed into an optical parametric amplifier (TOPAS). In both transient absorption and time-resolved experiments the light from the TOPAS was passed through a delay line and used as the pump laser. The residual 800 nm light from the pump beam was removed using a blue filter and the intensity was set below 2 μJ with optical density filters to reduce the probability of two-photon excitation. The remaining 800 nm light from the regenerative amplifier is passed through a delay line followed by white light generation in a 3 mm thick sapphire crystal. The white light continuum is then directed through the sample in a nearly colinear geometry to the pump beam, and into a Princeton Instruments TRY-700 diode array detector. A portion of the probe beam was split off and passed through the sample as the reference beam. In time-resolved experiments, the white light continuum passing through the sample coincident with the pump beam was passed through a monochromator and then directed into one photodiode of a Becker-Hickl dual integrating diode collection system. A portion of the probe beam was also passed through the sample and served as the reference beam. Alternatively, the data were collected as a series of transient absorption spectra using the diode array spectrometer and the data plotted using IgorPro. All kinetic results presented are averages of five independent measurements.

Nanosecond flash photolysis experiments

Nanosecond time-resolved absorption experiments were performed on a home-built laser flash photolysis system using the output from a Lambda-Physik Scanmate 2E dye laser pumped by a Spectra-Physics PRO-190 Nd:YAG laser. A pulsed Xe lamp was used as the white light source. Detection of transient absorption signals was accomplished using an Andor Instruments intensified charge-coupled device (ICCD), while time-resolved signals were collected through a monochromator into a Hamamatsu R5108 photomultiplier tube. The data from the time-resolved experiments was acquired on a 500 MHz digitizing oscilloscope and the transient absorption signals were then analyzed.

Electrochemistry

Cyclic voltammograms were recorded on a BAS-100 electrochemistry apparatus from Bioanalytical Systems, Inc. at 20 °C. A three-electrode configuration was used with platinum working and auxiliary electrodes, and a SCE reference electrode. The electrolytes used in all experiments were 0.1 M tetra-*n*-butyl ammonium hexafluorophosphate ($TBAPF_6$) for the Os-containing complexes or 0.1 M tetra-*n*-butyl ammonium perchlorate (TBAP) for the Ru-containing complexes. Ferrocene (Fc) was employed as an internal reference redox standard in all experiments, and all redox potentials are reported relative to the Fc^+/Fc couple. All electrochemical experiments were run at a concentration of 2.0×10^{-3} M in either spectroscopic grade CH_3CN (Os-containing complexes) or in freshly distilled DMF (Ru-containing complexes). Oxygen was removed by purging the stirred solutions with nitrogen; the samples were kept under a nitrogen atmosphere during all measurements.

Experimental procedures for the synthesis of 1–10, 12, 15, 16 and 18–20. *p*-Iodobenzaldehyde,[49] 4′-phenyl-2,2′:**6′**,2″-terphyridine (**11**),[50] 1-Bromo-2′,5′-dimethoxybiphenyl,[51] 2′,5′-dimethoxybiphenylboronic acid (**14**),[51] Os(4′-phenyl)-2,2′:**6′**,2″-terpyridine)$_2$-$(PF_6)_2$,[52] Ru(4′-phenyl)-2,2′:**6′**,2″-terpyridine)$_2(PF_6)_2$,[53] 1,4-bis(3-trifluoromethylphenyl)benzene-2,3,5,6-tetracarboxylic anhydride (**17**)[24] and 4′-(*para*-ethynylphenyl)-2,2′:**6′**,2″-terpyridine (**19**)[54] were synthesized according to literature procedures. 2-Acetylpyridine, 4-bromobenzaldehyde, 2,5-dimethoxyphenyl boronic acid, 4-iodo-1-bromobenzene and trimethylsilylacetylene were purchased from Fisher. Tetrakis palladium triphenylphosphine, ruthenium(III) chloride hydrate and osmium(III) chloride hydrate were purchased from Strem.

The synthetic procedures for **1–10**, **12**, **15**, **16** and **18–20** are described as follows.

4′-(*para*-Iodophenyl)-2,2′:6′,2″-terpyridine (12). To a solution of *p*-iodobenzaldehyde (2.00 g, 8.62 mmol) and 2-acetylpyridine (3.13 g, 25.8 mmol) in absolute ethanol (75 mL) was added NaOH (1 M, 6.88 mL) dropwise over 2 min. The reaction mixture was then stirred at room temperature overnight. The resulting solution was evaporated, and the resulting oil was taken up in 150 mL $CHCl_3$, washed twice with 150 mL water, dried over Na_2SO_4 and evaporated under reduced pressure. To the resulting residue was added ammonium acetate (22 g, 285 mmol) and 86 mL glacial acetic acid. The dark solution was refluxed for 4 h, and upon cooling the solution was neutralized with saturated $NaHCO_3$ to yield a yellow precipitate. The precipitate was filtered, washed with water and purified by column chromatography on alumina using 10% EtOAc/hexanes as the eluent to yield a white solid (1.16 g, 31%, mp 178–179 °C). ^{1}H NMR ($CDCl_3$, δ) 8.732 (d, 1H, J = 3.97), 8.711 (s, 1H), 8.667 (d, 1H, J = 8.09), 7.844 (m, 2H), 7.641 (d, 1H, J = 8.40), 7.351 (t, 1H).^{13}C NMR ($CDCl_3$, δ) 156.309, 156.249, 149.358, 138.283, 138.200, 137.130, 129.261, 124.154, 121.592, 118.697. HR ESI$^-$MS: m/z [M + H] = 436.030 (calcd for $C_{21}H_{14}N_3I$: 435.25).

General procedure for the 4′-(2′,5′-dimethoxybiphenyl)-2,2′:6′,2″-terpyridine (15) and 4′-(2′,5′-dimethoxyterphenyl)-2,2′:6′,2″-terpyridine (16) ligands. To a solution of **12** (0.35 g, 0.811 mmol) and the appropriate boronic acid (0.973 mmol) in DME (7 mL) was added K_2CO_3 (2 M, 1.1 mL) and $Pd(Ph_3P)_4$. The reaction was refluxed for 10 h. After cooling to room temperature, the solution was diluted with CH_2Cl_2 (20 mL) and the layers separated. The organic layer was washed with 10% NaOH, water and brine and dried over Na_2SO_4. The solvent was removed under reduced pressure, and the resulting yellow solid was purified by column chromatography on neutral alumina with a 25% EtOAc/hexanes mixture as the eluent to yield a white solid.

4′-(2′5′-Dimethoxybiphenyl)-2,2′:2″,6′-terpyridine (15). Terpyridine **15** was synthesized in 68% yield (0.25 g, mp 190–191 °C) using the general procedure for the DMB-Ph$_n$-tpy ligands and 2,5-dimethoxyphenylboronic acid. ^{1}H NMR ($CDCl_3$, δ) 8.814 (s, 2H), 8.75 (d, 2H, J = 4.73), 8.712 (s, 1H), 8.685 (s, 1H), 7.975 (d, 2H, J = 8.39), 7.899 (t, 2H), 7.693 (d, 2H, J = 8.24), 7.365 (m, 2H), 6.955 (m, 3H), 3.850 (s, 3H), 3.802 (s, 3H). ^{13}C NMR ($CDCl_3$, δ) 156.563, 156.153, 154.070, 151.111, 150.211, 149.286, 139.447, 137.083, 137.023, 130.231, 130.182, 127.215, 124.016, 121.584, 119.015, 116.853, 113.658, 113.081, 56.628, 56.066. HR ESI-MS: m/z [M + Na] = 468.167 (calcd for $C_{29}H_{23}N_3O_2$: 445.49).

4′-(2″5″-Dimethoxyterphenyl)-2,2′:2″,6′-terpyridine (16). Terpyridine **16** was synthesized in 64% yield (0.27 g, mp 178–179 °C) from **12** and **14** using the general procedure for the DMB-Ph$_n$-tpy ligands. ^{1}H NMR ($CDCl_3$, δ) 8.842 (s, 2H), 8.773 (d, 2H, J = 4.58), 8.736 (s, 1H), 8.710 (s, 1H), 8.034 (d, 2H, J = 8.09), 7.914 (t, 2H), 7.813 (d, 2H, J = 8.09), 7.750 (d, 2H, J = 8.09), 7.680 (d, 2H, J = 8.09), 7.390 (m, 2H), 6.968 (m, 3H), 3.861 (s, 3H), 3.829 (s, 3H). ^{13}C NMR ($CDCl_3$, δ) 156.478, 156.175, 154.004, 151.064, 149.967, 149.357, 141.764, 139.264, 137.985, 137.431, 137.056, 131.311, 130.162, 127.938, 127.737, 126.975, 124.026, 121.560, 118.878, 116.833, 113.444, 112.860, 56.532, 56.016. HR ESI-MS: m/z [M + H] = 522.218 (calcd for $C_{35}H_{27}N_3O_2$: 521.58).

General procedure for [Ru(4′-(2′,5′-dimethoxybiphenyl)-2,2′:6′,2″-terpyridine)$_2$][PF$_6$]$_2$ (1) and [Ru(4′-(2′,5′-dimethoxybiphenyl)-2,2′:6′,2″-terpyridine)$_2$][PF$_6$]$_2$ (2). To a suspension of the appropriate ligand in water (13 mL) and absolute ethanol (30 mL) was added $RuCl_3 \cdot 3H_2O$ (0.023 g, 0.112 mmol), and the reaction mixture refluxed for 15 h. Upon cooling, an aqueous solution of NH_4PF_6 (0.046 g) in 1.0 mL water was added. The precipitate was filtered and washed with water. Purification by column chromatography on neutral alumina using toluene:acetonitrile (100:0 to 0:100) as the eluent gave a red solid.

[Ru(4′-(2′,5′-dimethoxybiphenyl)-2,2′:6′,2″-terpyridine)$_2$][PF$_6$]$_2$ (1). Complex **1** was synthesized from **15** and $RuCl_3 \cdot 3H_2O$ in 63% yield (0.093 g). UV-Vis (λ, nm) 494, 311, 331sh. ^{1}H NMR ($(CD_3)_2CO$, δ) 9.522 (s, 2H), 9.117(d, 2H, J = 8.09), 8.353 (d, 2H, J = 8.24), 8.140(t, 2H), 7.917, (d, 2H, J = 8.24), 7.850 (d, 2H, J = 4.89), 7.380(t, 2H), 7.047 (m, 3H), 3.870 (s, 3H), 3.867(s, 3H). ^{13}C NMR ($(CD_3)_2CO$, δ) 159.635, 156.816, 153.618, 151.933, 149.152, 139.215, 136.111, 131.490, 128.762, 128.326, 125.795, 122.395, 117.528, 114.614, 114.147, 56.752, 56.100. ESI-MS m/z [M]$^{2+}$ = 496.2 (calcd for $[C_{58}H_{46}N_6O_4Ru]^{2+}$: 992.05).

[Ru(4′-(2′,5′-dimethoxyterphenyl)-2,2′:6′,2″-terpyridine)$_2$][PF$_6$]$_2$ (2). Complex **2** was synthesized from **16** and $RuCl_3 \cdot 3H_2O$ in 57% yield (0.093 g). UV-Vis (λ, nm) 495, 312, 333sh. ^{1}H NMR ($(CD_3)_2SO$, δ) 9.584 (s, 2H), 9.185 (d, 2H, J = 7.94), 8.610 (d, 2H, J = 8.39), 8.147 (m, 4 H), 7.986 (d, 2H, J = 8.40), 7.720 (d, 2H, J = 7.63), 7.595 (d, 2H, J = 4.73) 7.311 (t, 2H), 7.100 (m, 1 H), 6.985 (m, 2 H), 3.795 (s, 3H), 3.774 (s, 3H). ^{13}C NMR ($(CD_3)_2SO$, δ) 168.677, 156.854, 156.122, 153.656, 148.253, 139.234, 131.145, 129.320, 128.781, 127.514, 125.841, 122.285, 117.342, 114.037, 56.680, 56.054. ESI-MS m/z [M]$^{2+}$ = 572.22 (calcd for $[C_{70}H_{54}N_6O_4Ru]^{2+}$: 1144.24).

General procedure for [Ru(4′-(4-(2-cyclohexa-2′,5′-diene-1,4-dione)phenyl)-2,2′:6′,2″-terpyridine)$_2$][PF$_6$]$_2$ (5) and [Ru(4′-(4-(2-cyclohexa-2′,5′-diene-1,4-dione)biphenyl)-2,2′:6′,2″-terpyridine)$_2$][PF$_6$]$_2$ (6). A solution of **1** or **2** (0.500 mmol) in CH_2Cl_2 (2 mL) was cooled to −78 °C in a dry ice/acetone bath. BBr_3 (1.0 M in CH_2Cl_2, 5.00 mmol) was added dropwise and the reaction stirred for 2 h. The solution was cooled to 0 °C and 10 mL water was added. The resulting solid was filtered, washed with CH_2Cl_2 and dissolved in 2 mL methanol. DDQ (2.5 mmol) was added, and the solution stirred for 1 h at room temperature and then refluxed for 15 min. Upon cooling, the product was filtered and washed with water. Purification by flash chromatography on Act III alumina using 5% MeOH:CH_3CN as the eluent gave a dark red solid.

[Ru(4′-(4-(2-cyclohexa-2′,5′-diene-1,4-dione)phenyl)-2,2′:6′,2″-terpyridine)$_2$][PF$_6$]$_2$ (5). Quinone **5** was prepared from dimethoxybenzene-containing **1** in 54% yield (0.33 g). UV-Vis (λ, nm) 497, 312, 330sh. ^{1}H NMR ($(CD_3)_2SO$, δ) 9.617 (s, 2H), 9.2000 (d, 2H, J = 8.09), 8.590 (d, 2H, J = 8.24), 8.052 (m, 4H), 7.934 (d, 2H, J = 8.09), 7.569 (d, 2H, J = 5.19), 7.305 (t, 2H), 7.222, (s, 1H), 7.076 (m, 2H). ^{13}C NMR ($(CD_3)_2SO$, δ).

[Ru(4′-(4-(2-cyclohexa-2′,5′-diene-1,4-dione)biphenyl)-2,2′:6′,2″-terpyridine)$_2$][PF$_6$]$_2$ (6). Quinone **6** was prepared from dimethoxybenzene-containing **2** in 52% yield (0.36 g). UV-Vis (λ, nm) 496, 312, 330sh. ^{1}H NMR ($(CD_3)SO$, δ) 9.652 (s, 2H), 9.255(d, 2H, J = 7.79), 8.665 (d, 2H, J = 7.63), 8.152(d, 2H, J = 8.39),

8.055, (m, 4H), 7.737 (d, 2H, $J = 8.08$), 7.573 (d, 2H, $J = 5.49$), 7.309 (t, 2H), 7.033 (m, 3H). ^{13}C NMR ($(CD_3)_2SO$, δ) 165.318, 158.083, 155.131, 152.164, 150.012, 146.249, 144.682, 140.136, 138.065, 137.435, 136.247, 135.431, 132.525, 132.130, 131.797, 130.226, 128.541, 127.798, 127.483, 126.682, 125.153, 121.055.

General procedure for [Os(4′-(2′,5′-dimethoxybiphenyl)-2,2′:6′,2″-terpyridine)$_2$][PF$_6$]$_2$ (3) and [Os(4′-(2′,5′-dimethoxyterphenyl)-2,2′:6′,2″-terpyridine)$_2$][PF$_6$]$_2$ (4). To a suspension of the appropriate terpyridine (0.674 mmol) in ethylene glycol (34 mL) was added $OsCl_3 \cdot nH_2O$ (0.100 g, 0.337 mmol), and the reaction mixture was refluxed overnight. The dark solution was cooled to room temperature and 0.04M NH_4PF_6 (34 mL) was added. The resulting solid was filtered and rinsed with water (300 mL), ethanol (150 mL) and toluene (150 mL). The solid was further purified by column chromatography on silica using an eluent composed of 7:1:0.5 CH_3CN:saturated KNO_3:water, and was recovered from the fractions by the addition of 0.04M NH_4PF_6. The dark solid was then filtered and re-dissolved in CH_3CN for an additional counter-ion exchange by adding an equal volume of 0.04M NH_4PF_6 and allowing the solution to stand for 15 min. Three times the volume of water was then added, and the solution was allowed to stand for an additional 15 min. The product was filtered, rinsed with water, ethanol and ether and dried under vacuum.

[Os(4′-(2′,5′-dimethoxybiphenyl)-2,2′:6′,2″-terpyridine)$_2$][PF$_6$]$_2$ (3). Complexation of **15** with $OsCl_3 \cdot nH_2O$ yielded **3** in 58% yield (0.27 g). UV-Vis (λ, nm) 674, 498, 323, 291. ^{1}H NMR (CD_3CN, δ) 9.087 (s, 2H) 8.637 (d, 2H, $J = 8.08$); 8.207 (d, 2H, $J = 8.08$), 7.908 (d, 2H, $J = 7.47$), 7.789 (t, 4H) 7.312 (d, 2H, $J = 5.65$), 7.067 (m, 2H), 7.006 (m, 1H), 3.849 (s, 3H), 3.835 (s, 3H). ^{13}C NMR (CD_3CN, δ) 162.654, 161.098, 156.188, 155.008, 153.536, 152.000, 148.224, 141.808, 138.876, 135.817, 131.538, 128.810, 128.753, 125.778, 121.305, 117.742, 114.779, 114.119, 56.967, 56.455. ESI-MS m/z $[M]^{2+} = 540.8$ (calcd for $[C_{58}H_{46}N_6O_4Os]^{2+}$: 1081.18).

Os(4′-(2″,5″-dimethoxyterphenyl)-2,2′:6′,2″-terpyridine)$_2$][PF$_6$]$_2$ (4). Complexation of **16** with $OsCl_3 \cdot nH_2O$ yielded **4** in 42% yield (0.22 g). UV-Vis (λ, nm) 675, 499, 319, 292. ^{1}H NMR (CD_3CN, δ) 9.110 (s, 2H), 8.739 (d, 2H, $J = 8.09$), 8.294 (d, 2 H, $J = 7.78$), 8.104 (d, 2H, $J = 8.39$), 7.804 (m, 4H), 7.715 (d, 2H, $J = 8.24$), 7.324 (d, 2H, $J = 5.18$), 7.059 (m, 2H), 6.975 (m, 3H), 3.823 (s, 3H) 3.797 (s, 3H). ^{13}C NMR (CD_3CN, δ) 153.862, 139.182, 131.545, 130.016, 129.139, 129.002, 128.084, 126.085, 121.486, 117.814, 114.312. ESI-MS m/z $[M]^{2+} = 617.2$ (calcd for $[C_{70}H_{54}N_6O_4Os]^{2+}$: 1233.37).

General procedure for preparation of [Os(4′-(4-(2-cyclohexa-2′,5′-diene-1,4-dione)phenyl)-2,2′:6′,2″-terpyridine)$_2$][PF$_6$]$_2$ (7) and [Os(4′-(4-(2-cyclohexa-2′,5′-diene-1,4-dione)biphenyl)-2,2′:6′,2″-terpyridine)$_2$][PF$_6$]$_2$ (8). A solution of **3** or **4** (0.500 mmol) in CH_2Cl_2 (2 mL) was cooled to −78 °C in a dry ice/acetone bath. BBr_3 (1.0 M in CH_2Cl_2, 5.00 mmol) was added dropwise and the reaction stirred for 2 h. The solution was cooled to 0 °C and 10 mL water was added. The resulting solid was filtered, washed with CH_2Cl_2 and dissolved in 2 mL methanol. DDQ (2.5 mmol) was added, and the solution stirred 1 h at room temperature and then refluxed for 15 min. Upon cooling, the quinone precipitated and was filtered, washed with methanol and dried under vacuum.

[Os(4′-(4-(2-cyclohexa-2′,5′-diene-1,4-dione)phenyl)-2,2′:6′,2″-terpyridine)$_2$][PF$_6$]$_2$ (7). Quinone **7** was prepared in 47% yield from dimethoxybenzene-containing **3** (0.31 g). UV-Vis (λ, nm) 680, 501, 319, 292. ^{1}H NMR (CD_3CN, δ) 9.075 (s, 2H), 8.626 (d, 2H, $J = 8.09$), 8.245 (d, 2H, $J = 8.39$), 7.886 (d, 2H, $J = 8.24$), 7.797 (t, 2H), 7.305 (d, 2H, $J = 5.49$), 7.107 (m, 2H), 6.939 (m, 3H).^{13}C NMR (CD_3CN, δ) 161.254, 156.473, 153.897, 139.267, 138.633, 137.787, 134.619, 131.777, 129.448, 129.087, 126.094, 121.863.

[Os(4′-(4-(2-cyclohexa-2′,5′-diene-1,4-dione)biphenyl)-2,2′:6′,2″-terpyridine)$_2$][PF$_6$]$_2$ (8). Quinone **8** was prepared in 54% yield from dimethoxybenzene-containing **4** (0.39 g). UV-Vis (λ, nm) 677, 500, 318, 289. ^{1}H NMR ($(CD_3)_2SO$, δ) 9.603 (s, 2H), 9.172 (d, 2H, $J = 7.93$), 8.584 (d, 2H, $J = 8.24$), 8.190 (d, 2H, $J = 7.18$), 8.016 (m, 4H), 7.764 (d, 2H, $J = 7.94$), 7.478 (d, 2H, $J = 5.34$), 7.235 (t, 2H), 7.036 (m, 3H). ^{13}C NMR ($(CD_3)_2SO$, δ) 165.754, 159.785, 158.746, 154.716, 145.402, 144.096, 137.825, 137.445, 134.812, 132.160, 130.195, 128.665, 127.292, 126.761, 119.597.

Iodophenylpyromellitimide (18). To a solution of **17** (0.47 g, 0.15 mmol) in DMF (1.2 mL) was added octylamine (0.12 g, 0.15 mmol) and 4-iodoaniline (.020 g, 0.15 mmol). The reaction was refluxed for 12 h. Upon cooling, the solution was poured into water, extracted with ethyl acetate, dried over sodium sulfate, and the solvent was removed under reduced pressure. The resulting crude oil was purified by column chromatography on silica using 25% EtOAc/hexanes as the eluent. Concentration of the fractions yielded a pale yellow solid (0.12 g, 29%, mp 181–182 °C). ^{1}H NMR ($CDCl_3$, δ) 7.82 (m, 2 H), 7.77 (d, 4 H, $J = 8$), 7.68 (s, 4 H), 7.13 (d, 2 H, $J = 8$), 3.59 (t, 2 H, $J = 8$), 1.60 (m, 2 H), 1.24 (s, 10 H), 0.85 (t, 3 H). ^{13}C NMR ($CDCl_3$, δ) 165.0, 163.8, 138.4, 137.0, 135.1, 134.0, 132.8, 131.2, 130.6, 128.5, 128.1, 126.7, 136.5, 30.0, 31.8, 29.2, 29.1, 28.4, 27.0, 22.7, 14.2. IR (cm^{-1}) 2927, 1727, 1436, 1372, 1166, 1073, 801, 698, 646. HR ESI-MS m/z [M + Na] = 841.10 (calcd for $[C_{38}H_{29}N_2O_4IF_6]$: 818.52).

Terpyphenylacetylenephenylpyromellitimide (20). To a mixture of **18** (0.16 g, 0.20 mmol) and **19** (0.078 g, 0.24 mmol) in triethylamine (6 mL) was added $Pd(Ph_3P)_4$ (0.04 g, 0.057 mmol). The reaction mixture was heated to 65 °C and stirred for 15 h. The reaction was cooled to room temperature and diluted with ethyl acetate (20 mL), and then washed with water (2 × 20 mL). The solvent was removed under reduced pressure and the resulting solid was purified by column chromatography on alumina using 25% ethyl acetate/hexanes as the eluent. Concentration of the fractions yielded a pale yellow solid (0.08 g, 38%, mp 306 °C). IR (cm^{-1}) 2928, 2856, 1727, 1602, 1566, 1519, 1368, 1336, 1126, 1092, 793, 653, 628. ^{1}H NMR ($CDCl_3$, δ) 8.76 (s, 2 H), 8.71 (s, 2 H), 8.68 (s, 2 H), 7.91 (m, 4 H), 7.83 (m, 2 H), 7.77 (s, 2 H), 7.64 (m, 2 H), 7.40 (m, 2 H), 3.60 (t, 2 H, $J = 6$), 1.58 (m, 7 H), 1.25 (m, 5 H), 0.87 (m, 3 H). ^{13}C NMR ($CDCl_3$, δ) 163.9, 156.2, 152.1, 149.3, 137.1, 132.8, 123.4, 131.3, 128.5, 127.5, 126.8, 126.5, 126.3, 124.1, 121.6, 118.8, 98.7, 90.6, 39.0, 31.9, 29.2, 29.2, 28.4, 27.0, 22.7, 14.2. HR ESI-MS m/z [M + H] = 1024.33 (calcd for $[C_{61}H_{43}N_5O_4F_6]$: 1023.97).

Os(phtpy-PI)$_2^{2+}$ (9). The osmium-containing pyromellitimide complex **9** was synthesized by refluxing **20** (0.11 g, 0.11 mmol) with $OsCl_3 \cdot nH_2O$ (0.014 g, 0.053 mmol) in ethylene glycol (10 mL) for 24 h. Upon cooling, 0.04 M NH_4PF_6 (5 mL) was added to precipitate the crude product. The crude solid was filtered and

further purified by column chromatography on silica using 50:50 CH_2Cl_2:CH_3CN as the eluent. The dark band was collected and the solvent was removed by rotary evaporation to yield a black solid (24%, 32 mg). UV-Vis (λ, nm) 318, 363, 499, 677. ^{1}H NMR ($CDCl_3$, δ) 8.74 (s, 2 H), 8.68 (s, 1 H), 8.66 (s, 1 H), 7.92 (d, 2 H, $J = 8$), 7.82 (m, 2 H), 7.76 (m, 2 H), 7.66 (m, 3 H), 7.40 (d, 2 H, $J = 8$), 3.59 (t, 2 H, $J = 7$), 1.60 (s, 7 H), 1.23 (m, 5 H), 0.86 (m, 3 H). ^{13}C NMR ($CDCl_3$, δ) 200.74, 180.5, 163.9, 156.2, 149.3, 137.1, 135.1, 134.093, 132.9, 132.4, 131.35 128.5, 127.5, 126.6, 126.3, 124.1, 121.6, 118.9, 39.0, 31.9, 29.2, 29.2, 28.4, 27.0, 22.0, 14.2.

Ru(Phtpy-PI)$_2^{2+}$ (10). The ruthenium-containing pyromellitimide complex **10** was synthesized by refluxing **20** (0.13 g, 0.13 mmol) with $RuCl_3 \cdot nH_2O$ (0.010 g, 0.065 mmol) in ethylene glycol (10 mL) for 24 h. Upon cooling, 0.04 M NH_4PF_6 (5 mL) was added to precipitate the crude product. The crude solid was filtered and further purified by column chromatography on silica using 50/50 CH_2Cl_2/CH_3CN as the eluent. The dark red band was collected and the solvent was removed by rotary evaporation to yield a red solid (19%, 30 mg). UV-Vis (λ, nm) 315, 498. ^{1}H NMR ($(CD_3)_2CO$, δ) 8.74 (s, 2 H), 8.69 (s, 1 H), 8.66 (s, 1 H), 7.90 (d, 2 H, $J = 8$), 7.84 (m, 2 H), 7.77 (s, 2 H), 7.69 (m, 3 H), 7.37 (d, 2 H, $J = 8$), 3.59 (t, 2 H, $J = 7$), 1.61 (s, 7 H), 1.26 (m, 5 H), 0.86 (m, 3 H). ^{13}C NMR ($(CD_3)_2CO$, δ) 159.5, 156.8, 153.6, 139.2, 131.4, 130.5, 129.3, 129.0, 128.7, 125.8, 122.5, 122.0, 39.0, 31.8, 29.3, 29.2, 28.4, 27.0, 22.1, 14.2.

Conclusions

The use of osmium bisterpyridines in donor–acceptor complexes and their photoinduced electron transfer properties have been examined and compared to the analogous ruthenium-containing complexes. Two types of acceptor groups, a benzoquinone (BQ) and a pyromellitimide (PI), were used for each metal terpyridine donor. Charge separation was found to be facile in the Ru(II)-BQ dyads **5** and **6**, occurring on the picosecond time-scale, but did not occur in Ru(II)-PI dyad **9**, presumably as a result of either the low value of ΔG_{ET} (–0.06 eV) or the inherently short ^{3}MLCT lifetime (~1.5–5.0 ns). Photoinduced charge separation, on the other hand, was found to be quite efficient in both Os(II)-BQ (**7** and **8**) dyads and to a lesser extent, Os(II)-PI (**10**), with rate constants in the picosecond time-scale for the quinone-containing dyads and on the nanosecond time-scale for the pyromellitimide-containing dyad. Charge separation for both benzoquinone-containing dyads having *one* phenyl spacer group between the terpyridine and BQ groups (*i.e.*, **5** and **7**) was more rapid than charge recombination. The Ru dyad containing *two* phenyl spacer groups (**6**) showed more rapid charge recombination than separation, while k_{ET} and k_{CR} were comparable in Os dyad **8**. The reason for this difference is attributed to the different amounts of electronic coupling between the M(tpy)$_2^{2+}$ and BQ groups in the two sets of dyads. In **5** and **7**, the electronic coupling between the donor and acceptor is likely to be enhanced by rotation of the phenyl bridge in the ^{3}MLCT excited state, a process that would lead to the observation of the increased value of k_{ET}; rotation of the phenyl group back to the relaxed geometry decouples the two groups from one another, a process that would decrease in k_{CR}. The additional phenyl group in **6** and **8** insulates the donor and acceptor from one another, and phenyl group rotation in these dyads therefore has less effect on the electronic coupling matrix. In diimide-containing **10**, charge separation was found to be significantly slower (by 4–5 orders of magnitude) than **7–8**, probably as a result of the nearly thermoneutral free energy for ET in this dyad. This work demonstrates that Os-containing compounds can be incorporated into traditional donor–acceptor dyads using quinones or diimide acceptor groups, and photoinduced charge separation occurs efficiently and quite rapidly, particularly with readily reduced acceptors such as benzoquinone.

Acknowledgements

D.A.M. gratefully acknowledges the support of the National Science Foundation (NSF-532057 and NSF-9816260), the donors of the Petroleum Research Fund (ACS-PRF-38996-AC4,7), the Ohio Board of Regents and The University of Akron. E.A.A. thanks the U.S. Department of Education for a GAANN fellowship. C.D.S. thanks the Flexsys Corporation for a graduate fellowship.

References

1 For recent reviews of the events occurring in the photosynthetic reaction center and light-harvesting complex, see: (*a*) D. C. Arnett, C. C. Moser, P. L. Dutton and N. F. Scherer, *J. Phys. Chem. B*, 1999, **103**, 2014–2032; (*b*) T. Pullerits and V. Sundström, *Acc. Chem. Res.*, 1996, **29**, 381–389.
2 See, for example: (*a*) V. K. Yachandra, K. Sauer and M. P. Klein, *Chem. Rev.*, 1996, **96**, 2927–2950; (*b*) W. Rüttinger and G. C. Dismukes, *Chem. Rev.*, 1997, **97**, 1–24; (*c*) R. J. Debus, *Biochim. Biophys. Acta*, 1992, **1102**, 269–352.
3 See, for example: (*a*) M. R. Wasielewski, *Chem. Rev.*, 1992, **92**, 435–461; (*b*) D. Gust and T. A. Moore, *Science*, 1989, **244**, 35–41; (*c*) T. J. Meyer, *Acc. Chem. Res.*, 1989, **22**, 163; (*d*) *Photoinduced Electron Transfer, Parts A-D*, ed. M.A. Fox and M. Chanon, Elsevier Science Publishers B.V., Amsterdam, 1988.
4 P. F. Barbara, T. J. Meyer and M. A. Ratner, *J. Phys. Chem.*, 1996, **100**, 13148–13168.
5 P. Lainé, F. Bedioui, P. Ochsenbein, V. Marvaud, M. Bonin and E. Amouyal, *J. Am. Chem. Soc.*, 2002, **124**, 1364.
6 B. O'Regan and M. Graetzel, *Nature*, 1991, **353**, 737; V. Balzani, S. Campagna, G. Denti, A. Juris, S. Serroni and M. Venturi, *Acc. Chem. Res.*, 1998, **31**, 26–34.
7 See, for example: (*a*) J. P. Sauvage, J. P. Collin, J. C. Chambron, S. Guillerez, C. Coudret, V. Balzani, F. Barigelletti, L. Decola and L. Flamigni, *Chem. Rev.*, 1994, **94**, 993–1019; (*b*) V. Balzani, A. Juris, M. Venturi, S. Campagna and S. Serroni, *Chem. Rev.*, 1996, **96**, 759.
8 C.-C. Chu and D. M. Bassani, *Photochem. Photobiol. Sci.*, 2008, **7**, 521–530; I. Ciofini, P. P. Laine, F. Bedioui and C. Adamo, *J. Am. Chem. Soc.*, 2004, **126**, 10763–10777.
9 S. Vaduvescu and P. G. Potvin, *Eur. J. Inorg. Chem.*, 2004, 1763–1769.
10 E. Baranoff, J.-P. Collin, L. Flamigni and J.-P. Sauvage, *Chem. Soc. Rev.*, 2004, **33**, 147–155; A. Harriman, M. Hissler, A. Khatyr and R. Ziessel, *Eur. J. Inorg. Chem.*, 2003, 955–959; P. A. Anderson, F. R. Keene, T. J. Meyer, J. A. Moss, G. F. Strouse and J. A. Treadway, *J. Chem. Soc., Dalton Trans.*, 2002, 3820–3831.
11 N. Sutin, *Acc. Chem. Res.*, 1982, **15**, 275.
12 L. De Cola, V. Balzani, F. Barigelletti, L. Flamigni, P. Belser, A. von Zelewsky, M. Frank and F. Vögtle, *Inorg. Chem.*, 1993, **32**, 5228; R. C. Young, J. K. Nagle, T. J. Meyer and D. G. Whitten, *J. Am. Chem. Soc.*, 1978, **100**, 4773–4778.
13 A. Juris, V. Balzani, F. Barigelletti, S. Campagna, P. Belser and A. von Zelewsky, *Coord. Chem. Rev.*, 1988, **84**, 85.
14 V. Balzani and A. Juris, *Coord. Chem. Rev.*, 2001, **211**, 97; E. C. Constable, *Chem. Commun.*, 1997, 1073.
15 E. C. Constable, E. L. Dunphy, C. E. Housecroft, W. Kylberg, M. Neuburger, S. Schaffner, E. R. Schofield and C. B. Smith, *Chem.–Eur. J.*, 2006, **12**, 4600–4610.
16 L. Flamigni, F. Barigelletti, N. Armaroli, J.-P. Collin, J.-P. Sauvage and J. A. G. Williams, *Chem.–Eur. J.*, 1998, **4**, 1744–1754.

17 M. Maestri, N. Armaroli, V. Balzani, E. C. Constable and A. M. W. C. Thompson, *Inorg. Chem.*, 1995, **34**, 2759.
18 O. Johansson, M. Borgström, R. Lomoth, M. Palmblad, J. Bergquist, L. Hammarström, L. Sun and B. Åkermark, *Inorg. Chem.*, 2003, **42**, 2908–2918.
19 C. M. Kober, B. P. Sullivan, W. J. Dressick, J. V. Caspar and T. J. Meyer, *J. Am. Chem. Soc.*, 1980, **102**, 7383; J.-P. Collin, S. Guillerez and J.-P. Sauvage, *Inorg. Chem.*, 1990, **29**, 5009.
20 G. R. Newkome, T. J. Cho, C. N. Moorefield, G. R. Baker, R. Cush and P. S. Russo, *Angew. Chem., Int. Ed.*, 1999, **38**, 3717–3721.
21 F. Bobe, A. R. Tunoori, A. J. Niestroj, O. Gronwald and M. E. Maier, *Tetrahedron*, 1996, **52**, 9485.
22 M. Beley, J.-P. Collin, J.-P. Sauvage, H. Sugihara, F. Heisel and A. Miehé, *J. Chem. Soc., Dalton Trans.*, 1991, **11**, 3157–3159.
23 B. Whittle, N. S. Everest, C. Howard and M. D. Ward, *Inorg. Chem.*, 1995, **34**, 2025–2032.
24 M. Tomikawa, F. W. Harris, S. Z. D. Cheng and E. Galentier, *React. Funct. Polym.*, 1996, **30**, 101–107.
25 V. Grosshenny, F. M. Romero and R. Ziessel, *J. Org. Chem.*, 1997, **62**, 1491–1500.
26 S. Takahashi, Y. Kuroyama, K. K. Sonogashira and N. Hagihara, *Synthesis*, 1980, 627–630.
27 A similarly red-shifted singlet MLCT band at λ_{MLCT} ~667–671 nm has been reported for 4′-biphenyl-2,2′;6′,2″-terpyridine. See: N. W. Alcock, P. R. Barker, J. M. Haider, M. J. Hannon, C. L. Painting, Z. Pikramenou, E. A. Plummer, K. Rissanen and P. Saarenketo, *J. Chem. Soc., Dalton Trans.*, 2000, **24**, 1447–1461.
28 G. L. Closs, L. T. Calcaterra, N. J. Green, K. W. Penfield and J. R. Miller, *J. Phys. Chem.*, 1986, **90**, 3673; L. T. Calcaterra, G. L. Closs and J. R. Miller, *J. Am. Chem. Soc.*, 1983, **105**, 670; M. N. Paddon-Row, *Acc. Chem. Res.*, 1994, **27**, 18; A. M. Oliver, D. C. Craig, M. N. Paddon-Row, J. Kroon and J. W. Verhoeven, *Chem. Phys. Lett.*, 1988, **150**, 366; J. M. Lawson, D. C. Craig, M. N. Paddon-Row, J. Kroon and J. W. Verhoeven, *Chem. Phys. Lett.*, 1989, **164**, 120.
29 C. S. Rajesh, G. J. Capitosti, S. C. Cramer and D. A. Modarelli, *J. Phys. Chem. B*, 2001, **105**, 10175–10188; G. J. Capitosti, S. C. Cramer, C. S. Rajesh and D. A. Modarelli, *Org. Lett.*, 2001, **3**, 1645–1648.
30 Estimated using the Weller equation ($\Delta G_{ET} = E_{ox} - E_{red} - e^2/\varepsilon r_{12} - E^*$) from the values recorded above. In this equation, e is the fundamental charge and r_{12} represents the donor–acceptor charge-separation distance of 11.9 Å (for **5** and **7**) or 16.3 Å (for **6** and **8**). A value of 35.94 was used for the dielectric constant for CH_3CN (see Scaiano, J. C. in *Handbook of Organic Photochemistry*, CRC Press, Inc., Boca Raton, FL, 1989, pp. 344 and 367 for DMF.
31 Y. Tachibana, J. E. Moser, M. Grätzel, D. R. Klug and J. R. Durrant, *J. Phys. Chem.*, 1996, **100**, 20056–20062.
32 N. H. Damrauer, G. Cerullo, A. Yeh, T. R. Boussie, C. V. Shank and J. K. McCusker, *Science*, 1997, **275**, 54–57.
33 D. Kuciauskas, J. E. Monat, R. Villahermosa, H. B. Gray, N. S. Lewis and J. K. McCusker, *J. Phys. Chem. B*, 2002, **106**, 9347–9358.
34 Time-resolved spectra at 515 and 600 nm for this spectrum are contained in the ESI.† Similarly, overlaid transient absorption spectra for **5**, as well as the corresponding time-resolved spectra (515 and 600 nm), are also contained in the ESI†.
35 A. C. Benniston, G. M. Chapman, A. Harriman and S. A. Rostron, *Inorg. Chem.*, 2005, **44**, 4029–4036.
36 L. M. Vogler, B. Scott and K. J. Brewer, *Inorg. Chem.*, 1993, **32**, 898–903; L. M. Vrana and K. J. Brewer, *J. Photochem. Photobiol. A*, 1997, **109**, 201–211.
37 S. W. Jones, L. M. Vrana and K. J. Brewer, *J. Organomet. Chem.*, 1998, **554**, 29–40.
38 Time-resolved spectra at 430, 520 and 600 nm for this spectrum are contained in the ESI.† Similarly, overlaid transient absorption spectra for **8**, as well as the corresponding time-resolved spectra (430, 520 and 600 nm), are also contained in the ESI†.
39 A. R. Cook, L. A. Curtiss and J. R. Miller, *J. Am. Chem. Soc.*, 1997, **119**, 5729–5734; T. Shida, *Electronic, Absorption Spectra of Radical Ions*, Elsevier Science Publishing Company, Inc., New York, 1988, vol. 34, pp. 308–312.
40 M. Falkenström, S. Ott, R. Lomoth, J. Bergquist, L. Hammarström and O. Johansson, *Inorg. Chem.*, 2006, **45**, 4820–4829; M. Falkenström, O. Johansson and L. Hammarström, *Inorg. Chim. Acta*, 2007, **360**, 741–750.
41 K. Yamada, H. Imahori, E. Yoshizawa, D. Gosztola, M. R. Wasielewski and Y. Sakata, *Chem. Lett.*, 1999, 235–236.
42 H. Suzuki, *Bull. Chem. Soc. Jpn.*, 1959, **32**, 1340; R. J. Kurland and W. B. Wise, *J. Am. Chem. Soc.*, 1964, **86**, 1877–1879; V. J. Eaton and D. Steele, *J. Chem. Soc., Faraday Trans. 2*, 1973, **69**, 1601; E. C. Lim and Y. H. Li, *J. Chem. Phys.*, 1970, **52**, 6416; H. Uchimura, A. Tajiri and M. Hatano, *Chem. Phys. Lett.*, 1975, **34**, 34; H. Uchimura, A. Tajiri and M. Hatano, *Bull. Chem. Soc. Jpn.*, 1981, **54**, 3279.
43 O. Bastiansen and S. Samdal, *J. Mol. Struct.*, 1985, **128**, 59, 95, 115; O. Bastiansen, *Acta Chem. Scand.*, 1949, **3**, 408.
44 Y. Takei, T. Yamaguchi, Y. Osamura, K. Fuke and K. Kaya, *J. Phys. Chem.*, 1988, **92**, 577–581; R. Li and E. C. Lim, *J. Chem. Phys.*, 1972, **57**, 605–612.
45 N. H. Damrauer, B. T. Weldon and J. K. McCusker, *J. Phys. Chem. A*, 1998, **102**, 3382–3397.
46 R. J. Cave, S. J. Klippenstein and R. A. Marcus, *J. Chem. Phys.*, 1986, **84**, 3089–3098.
47 A. Osuka, J.-Y. Shin, R. Yoneshima, H. Shiratori, T. Ohno, K. Nozaki, Y. Nishimura, I. Yamazaki, S. Taniguchi, T. Shimizu and T. Okada, *J. Porphyrins Phthalocyanines*, 1999, **3**, 729–741; A. Helms, D. Heiler and G. McLendon, *J. Am. Chem. Soc.*, 1991, **113**, 4325–4327.
48 It should be noted that the phenyl rotation probably occurs to an equal extent in dyads **5–8**, but the additional phenyl group between the $M(tpy)_2^{2+}$ and BQ groups in **6** and **8** in all likelihood minimizes the enhancement in the electronic coupling that occurs in dyads **5** and **7**. Charge recombination is more exergonic than charge separation in all four dyads, and the relative energies of CR/CS probably become more important in **6** and **8** than the more minor changes in electronic coupling induced by the presence of the second phenyl group. As a result, charge recombination becomes more rapid than charge separation in **6** and **8**, despite the excited state structural changes.
49 P. T. Sah, *J. Am. Chem. Soc.*, 1942, **64**, 1487–1488.
50 E. C. Constable, J. Lewis, M. C. Liptrot and P. R. Raithby, *Inorg. Chim. Acta*, 1990, **178**, 47–54.
51 G. J. Capitosti, C. D. Guerrero, D. E. Binkley, Jr., C. S. Rajesh and D. A. Modarelli, *J. Org. Chem.*, 2003, **68**, 247–261.
52 K. Chichak and N. Branda, *Chem. Commun.*, 1999, 523–524.
53 R. P. Thummel, V. Hegde and Y. Jahng, *Inorg. Chem.*, 1989, **28**, 3264–3267.
54 V. Grosshenny, F. M. Romero and R. Zeissel, *J. Org. Chem.*, 1997, **62**, 1491–1500.